Aerosol impacts on clouds and precipitation in eastern China: Results from bin and bulk microphysics

Jiwen Fan,[1] L. Ruby Leung,[1] Zhanqing Li,[2] Hugh Morrison,[3] Hongbin Chen,[4] Yuquan Zhou,[5] Yun Qian,[1] and Yuan Wang[6]

Received 14 July 2011; revised 18 November 2011; accepted 22 November 2011; published 19 January 2012.

[1] Using the Weather Research and Forecasting model coupled with a spectral-bin microphysics ("SBM") and measurements from the Atmospheric Radiation Measurement Mobile Facility field campaign in China (AMF-China), the authors examine aerosol indirect effects (AIE) in the typical cloud regimes of the warm and cold seasons in Southeast China: deep convective clouds (DCC) and stratus clouds (SC), respectively. Comparisons with a two-moment bulk microphysics ("Bulk") are performed to gain insights for improving bulk schemes in estimating AIE in weather and climate simulations. For the first time, measurements of aerosol and cloud properties acquired in China are used to evaluate model simulations to better understand aerosol impact on clouds in the southeast of China. It is found that changes in cloud condensation nuclei (CCN) concentration significantly change the timing of storms, the spatial and temporal distributions of precipitation, the frequency distribution of precipitation rate, as well as cloud base and top heights for the DCC, but not for the SC. Increasing CCN increases cloud droplet number (N_c) and mass concentrations, decreases raindrop number concentration, and delays the onset of precipitation. Compared with SBM, Bulk predicts much higher N_c and the opposite CCN effects on convection and heavy rain, stemming from the fixed CCN prescribed in Bulk. CCN have a significant effect on ice microphysical properties with SBM but not Bulk and different condensation/deposition freezing parameterizations employed could be the main reason. This study provided insights to further improve the bulk scheme to better account for aerosol-cloud interactions in regional and global climate simulations, which will be the focus for a follow-on paper.

Citation: Fan, J., L. R. Leung, Z. Li, H. Morrison, H. Chen, Y. Zhou, Y. Qian, and Y. Wang (2012), Aerosol impacts on clouds and precipitation in eastern China: Results from bin and bulk microphysics, *J. Geophys. Res.*, *117*, D00K36, doi:10.1029/2011JD016537.

1. Introduction

[2] Many observational and modeling studies have indicated that aerosols may significantly affect convection and cloud properties [e.g., *Rosenfeld*, 2000, *Andreae et al.*, 2004, *Koren et al.*, 2008, *Khain et al.*, 2005], with a great potential to affect the radiative forcing of the atmosphere and hydrological cycle. Yet, aerosol indirect effects (AIE), the effects of aerosols acting as cloud condensation nuclei (CCN) or ice nuclei (IN), remain one of the least understood aspects of climate science [*National Research Council*, 2005], as it is difficult to establish clear causal relationships between aerosols and precipitation and to determine the sign of precipitation change in a climatological sense [*Levin and Cotton*, 2008]. AIE could be very different for different types of clouds. For warm stratiform clouds, although relatively consistent results have been reached for aerosol effects on droplet number concentration and cloud albedo [e.g., *Kaufman et al.*, 2005], there is still a large uncertainty on aerosol impact on liquid water path and precipitation, depending on dynamics-microphysics feedbacks [e.g., *Ackerman et al.*, 2004; *Guo et al.*, 2008]. For deep convective clouds (DCC) where both dynamics and thermodynamics and their interactions are important [*Rosenfeld et al.*, 2008; *Tao et al.*, 2007; *Khain et al.*, 2009], AIE become much more complicated: it may suppress convection and precipitation [*Rosenfeld*, 2000; *Khain et al.*, 2004; *Khain and Pokrovsky*, 2004] or vice versa [*Khain et al.*, 2005; *Fan et al.*, 2007b; *Lin et al.*, 2006; *van den Heever et al.*, 2006; *Zhang et al.*, 2007], depending on

[1]Atmospheric Sciences and Global Change Division, Pacific Northwest National Laboratory, Richland, Washington, USA.
[2]Department of Atmospheric and Oceanic Sciences, University of Maryland, College Park, Maryland, USA.
[3]Mesoscale and Microscale Meteorology Division, National Center for Atmospheric Research, Boulder, Colorado, USA.
[4]Institute of Atmospheric Physics, Chinese Academy of Sciences, Beijing, China.
[5]Weather Modification Centre, Chinese Academy of Meteorological Sciences, Beijing, China.
[6]Department of Atmospheric Sciences, Texas A&M University, College Station, Texas, USA.

0148-0227/12/2011JD016537

environmental conditions [*Khain et al.*, 2008]. Wind shear is found to be the determining factor in suppressing/enhancing convection for isolated DCC [*Fan et al.*, 2009b]. While many previous studies concerning these effects are based on model simulations and/or individual cases, *Li et al.* [2012] revealed long-term (10 years) aerosol effects of both suppressing and enhancement of cloud vertical development and precipitation.

[3] China has been the most populated and rapidly developing region in the world during the last few decades. The ever-growing population and human activities have led to a rapid and continued increase in emissions of aerosols and their precursors [*Qian et al.*, 2006], which has substantially altered the radiation budget at the surface and in the atmosphere [*Li et al.*, 2007, 2010] and heating rate of the atmosphere [*Liu et al.*, 2012]. Decadal increases in aerosols were speculated as one of the factors affecting changes of precipitation in China [*Cheng et al.*, 2005; *Zhao et al.*, 2006; *Qian et al.*, 2003, 2009]. Fewer studies have investigated aerosol indirect effects due to the dearth of in situ measurements of coincident aerosol and cloud properties in China. Observations from satellite [*Yuan et al.*, 2008] and surface measurements [*Rosenfeld et al.*, 2007] were employed to study AIE in China. However, determining AIE from observations is difficult because of the issue of correlation versus causation and confounding factors like meteorology [*Loeb and Schuster*, 2008; *Stevens and Feingold*, 2009]. There are also limitations in studying AIE in-depth by empirical relationships of droplet concentrations, droplet radius or precipitation with aerosol concentrations employed in the previous modeling studies of AIE in China [e.g., *Qian et al.*, 2003; *Huang et al.*, 2007] since feedbacks between dynamics and microphysics cannot be accounted for. More recently, AIE in China were studied using spectral-bin cloud microphysics [*Qian et al.*, 2009; *Iguchi et al.*, 2008]. However, the lack of in situ measurements of cloud properties in China limited in-depth investigations of AIE.

[4] To fill the gap in our understanding of aerosol effects, the U.S. Department of Energy (DOE) Atmospheric Radiation Measurement (ARM) Mobile Facility (AMF) was deployed in China to study AIE. The field campaign, named AMF-China, was designed to collect a comprehensive data set that can be used to study the impact of heavy aerosol loading on radiative fluxes, clouds, and precipitation, as well as the general climate in China and downstream regions [*Li et al.*, 2011]. AMF-China deployed instruments at a few sites in China from May to December, 2008. The primary AMF site was located at Shouxian, approximately 500 km west of Shanghai in southeastern China (SEC). Aerosol and cloud properties measured by this campaign provide key observations for evaluating models and allowing us to examine aerosol impacts on cloud microphysical properties and precipitation.

[5] Cloud microphysical processes are generally represented in models using a bulk approach or a bin approach. In bulk schemes, hydrometeor size distributions are diagnosed from the predicted (average) mass (one-moment schemes) or number and mass (two-moment schemes) of the hydrometeors and an assumed spectral shape (e.g., gamma function). In bin schemes, the size distributions of aerosols and cloud hydrometeors are discretized by a number of size bins and predicted, which is very important to study AIE [*Iguchi et al.*, 2008]. Many studies have indicated that the bin approach reproduces more realistic cloud structures and convection and predict precipitation in better agreement with the observations [*Lynn et al.*, 2005a, 2005b; *Khain et al.*, 2009; *Iguchi et al.*, 2008] and bin simulations have been used as benchmarks to adjust and improve the bulk schemes [e.g., *Seifert et al.*, 2006]. However, due to large computational cost, most bin schemes have been applied only in two-dimensional (2-D) runs [*Khain et al.*, 2005; *Tao et al.*, 2007; *Fan et al.*, 2007a, 2007b] or in 3-D warm cloud simulations excluding ice microphysical processes [*Feingold and Kreidenweis*, 2002]. With advances in computational power in recent years, 3-D simulations have been conducted with the bin schemes for DCC at the cloud-resolving scale [*Iguchi et al.*, 2008; *Fan et al.*, 2009a, 2010a, 2010b]. However, for regional or global climate simulations, bulk schemes are the only computationally feasible approach. To reduce uncertainty in estimating AIE in climate simulations, bulk schemes should be extensively evaluated.

[6] In this study, we perform real-case simulations of typical cloud regimes during the warm and cold seasons in Southeast China: deep convective clouds (DCC) and stratus clouds (SC), respectively, using the Weather Research and Forecasting (WRF) Model [*Skamarock et al.* 2005] coupled with an explicit bin microphysics parameterization based on work by *Khain et al.* [2004]. The simulated DCC and SC were observed at Shouxian during the AMF-China field campaign on July 16–18 and November 5–7 in 2008, respectively. The simulated cloud system, cloud microphysical properties, and precipitation have been compared with the retrieved space and ground-based remote sensing data and rain gauge data. Sensitivity studies are performed by changing aerosol concentrations to explore AIE on cloud properties and precipitation. The significance of AIE for different cloud systems is addressed. The simulated cloud systems and AIE based on the bin scheme are extensively compared with those with a two-moment bulk microphysics scheme [*Morrison et al.*, 2005, 2009], with the purpose of gaining insights for improving cloud microphysical representations and reducing uncertainty associated with AIE in cloud and climate simulations. To show how results from the bulk scheme in WRF are different from those using the SBM and to identify areas for improvement of the bulk scheme, we start with the scheme of *Morrison et al.* [2005, 2009] in which the background CCN properties are assumed to be constant.

2. Case Descriptions

2.1. Deep Convective Clouds (DCC)

[7] Strong thunderstorms were observed at Shouxian, Anhui province, in the late afternoon of July 17, 2008. The thunderstorms formed when the NW-SE oriented cool flow from the north encountered the NE-SW oriented monsoon trough and the associated warm and humid air over the Henan and Anhui provinces (Shouxian is located in the middle of Anhui Province), producing strong precipitation. At 10:00 UTC (18:00 LST) of July 17, the combined flow moved over the Shouxian region. Driven by solar heating in addition to atmospheric instability due to the large-scale meteorology, strong thunderstorms formed at Shouxian, resulting in 81.7 mm of rainfall at the surface. Figure 1a shows the satellite image of the cloud system from the

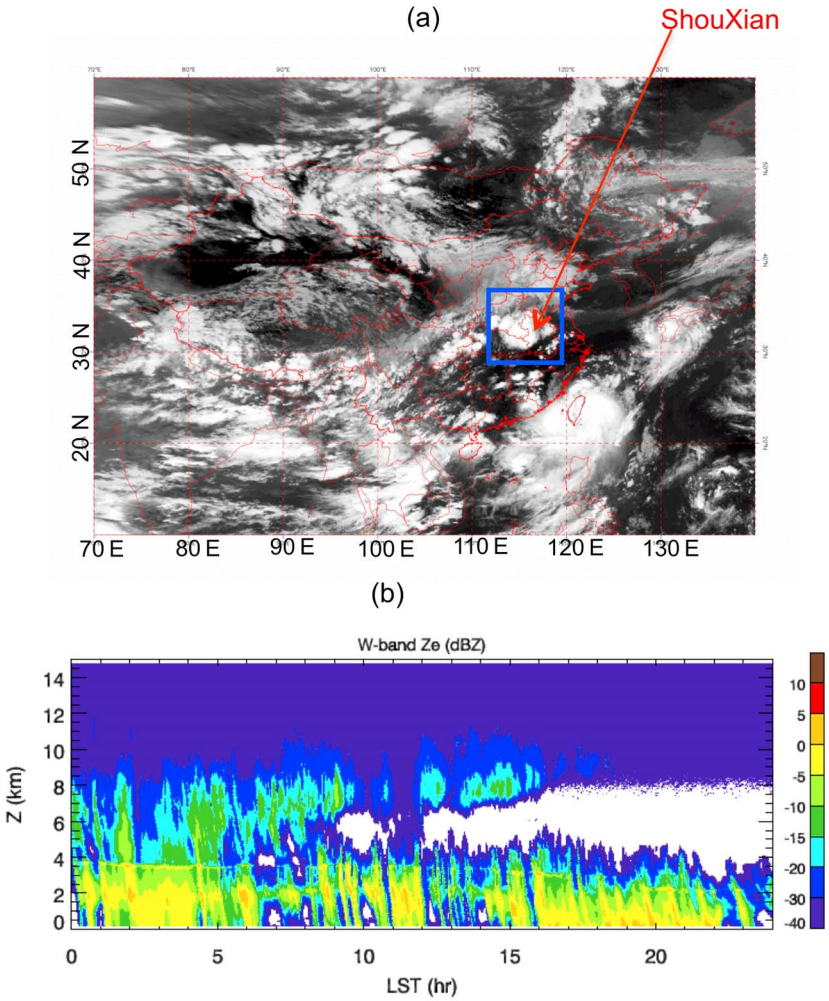

Figure 1. (a) Image of the developing DCC storm at about 17:00 LST, July 17 from the Multifunctional Transport Satellites (MTSAT), and (b) the radar reflectivity from the W-band ARM Cloud Radar (WACR) at the Shouxian (SX) site for the SC.

Multifunctional Transport Satellites (MTSAT), about one hour before the maximum precipitation rate at Shouxian, showing a big storm system over Henan and Anhui provinces that was developing (in the blue box).

2.2. Stratus Clouds (SC)

[8] The nimbostratus and stratus clouds formed on November 17 at the Shouxian region were associated with the passage of a cold front that moved from the northwest to the southeast of China and passed over the Anhui Province. The W-band (95 GHz) ARM Cloud Radar (WACR) was operating and captured this cloud event (WACR did not operate before October 2008). Although the retrieved cloud properties from these radar measurements are not available yet, the measured radar reflectivity can give us some basic idea of the cloud structure. The radar reflectivity from WACR at the Shouxian site shows the time evolution of the cloud system (Figure 1b). The cold front arrived at Shouxian at about 0:00 LST on Nov 07 and precipitation began. The rain lasted for about 4 h and the accumulated precipitation reached about 0.8 mm. The clouds were then separated into two layers: upper ice clouds and lower mostly liquid clouds. The stratiform clouds produced relatively more precipitation than the previous period, with accumulated surface rainfall of about 2.3 mm. At 12:00 UTC on Nov 07, the SC began to dissipate. Overall, the SC over the Shouxian region lasted for about one day.

3. Model Description and Designs of Numerical Experiments

[9] Simulations have been performed using WRF version 3.1.1 developed at the National Center for Atmospheric Research (NCAR) [*Skamarock et al.*, 2005]. WRF solves the fully compressible, nonhydrostatic Euler equations formulated on the terrain following hydrostatic-pressure vertical coordinate and the Arakawa C-grid. The model uses the Runge-Kutta second- and third-order time integration schemes, and second- to sixth-order advection schemes in both horizontal and vertical directions [*Li et al.*, 2008]. The 5-th order advection scheme is used in this study. The positive definite technique is employed for advection of scalar variables. The microphysical schemes used in the study are briefly described below.

3.1. Spectral-Bin Microphysics (SBM)

[10] The spectral bin microphysics (SBM) scheme used in this study is based on the Hebrew University Cloud Model (HUCM) described by *Khain et al.* [2004], *Lynn and Khain* [2007], and *Khain et al.* [2009]. The microphysics parameterization solves a system of kinetic equations for the size distribution functions for water drops, ice crystals (plate, columnar and branch types), snow/aggregates, graupel and hail/frozen drops, as well as CCN. Each size distribution is represented by 33 mass doubling bins, i.e., the mass of a particle m_k in the k bin is determined as $m_k = 2m_{k-1}$. The CCN size distribution is prognostic with sinks and sources, which include advection, nucleation, and CCN regeneration from droplet evaporation [*Fan et al.*, 2009a]. Scavenging of CCN by precipitation is not considered. All relevant cloud microphysical processes/interactions including droplet nucleation, primary and secondary ice generation, condensation/evaporation of drops, deposition/sublimation of ice particles, freezing/melting, and mutual collisions between the various hydrometeors are calculated explicitly. The model accounts for the dependence of the collision efficiencies on height, as well as effects of turbulence on the rate of collisions [*Pinsky and Khain*, 1998; *Pinsky et al.*, 2000]. Droplet nucleation is calculated according to the Köhler theory for each CCN bin. Equilibrium is assumed for CCN of radius (r_N) < 0.03 μm to calculate newly formed droplet size; for larger CCN (i.e., r_N > 0.03 μm), the formed droplet size is a factor of 3–8 that of the dry CCN size (a factor of 5 is used in this study) [*Khain and Lynn*, 2009], since these particles grow much faster (probably requires time step <0.001 s to calculate equilibrium) [*Kogan*, 1991]. The model employs the parameterization of Meyers *et al.* [1992] for condensation/deposition freezing and *Bigg* [1953] for drop freezing (i.e., immersion and homogeneous freezing). Aerosol homogeneous freezing is not considered in this study. Table 1 summarizes the droplet and ice nucleation parameterizations used by SBM. More details about the bin scheme is provided by *Khain et al.* [2010]. The model is especially designed to take into account the effects of aerosols on cloud microphysics, dynamics, and precipitation by serving as CCN.

[11] Since the full SBM is highly computationally expensive, especially when it is coupled with WRF and run three dimensionally, a Fast-SBM has been developed and applied to WRF [*Khain et al.*, 2009, 2010]. In the Fast-SBM, all ice crystals and snow (aggregates) are calculated on one size distribution. The smaller ice particles with sizes less than 150 micron are assumed to be crystals, while larger particles are assigned to snow. Graupel and hail in the full version are grouped to be the high-density ice, represented with one size distribution without separation. No changes in the microphysical processes have been made compared to the full SBM. As a result, the number of size distributions decreases from eight to four (aerosols, water drops, low-density ice, high-density ice). Since Fast-SBM keeps the main advantages of the full SBM, it produces cloud microphysical and dynamical structure as well as precipitation similar to the full SBM [*Khain et al.*, 2009].

[12] The WRF model with the Fast-SBM has been extensively tested and improved for this study. The new remapping scheme applied to diffusion growth/evaporation [*Khain et al.*, 2008; *Fan et al.*, 2009a] has been further improved to significantly reduce artificial numerical droplet spectrum broadening. We also have added a diagnostic CCN approach to the scheme (i.e., the sum of droplet and CCN concentration never exceeds the initial total CCN concentration) for places where aerosol sources are prescribed, to avoid unrealistic droplet nucleation in the source regions.

3.2. Two-Moment Bulk Microphysics

[13] We conduct an intercomparison of the results between the SBM and a two-moment cloud microphysical scheme, with the purpose of gaining insights for improving bulk schemes that have been widely used in cloud and climate simulations. We choose the Morrison two-moment scheme, referred to as "Bulk" [*Morrison et al.*, 2005; *Morrison and Pinto*, 2005], because it is widely used and includes the power law CCN distribution that SBM also employs [*Khain et al.*, 2004]. The power law function is expressed as [*Pruppacher and Klett*, 1997]

$$N_{ccn} = cS_w{}^k \tag{1}$$

where S_w is the supersaturation with respect to water, and c and k are parameters that depend on the air mass type. Droplet activation for the power law CCN spectrum follows *Twomey* [1959], which is

$$Nc \approx 0.88c^{2/(k+2)}\left[0.07w^{3/2}\right]^{k/(k+2)} \tag{2}$$

where N_c is droplet number in cm^{-3} and w is updraft velocity in cm s^{-1} [*Rogers and Yau*, 1989]. In this formulation, droplet activation is tied to the fixed parameters c and k. Since there is no way to predict c and k during simulations and these are just empirical parameters, this formulation of droplet activation cannot be extended to a prognostic CCN scheme. To prevent "runaway" nucleation with the fixed CCN, in-cloud nucleation scavenging is treated so that the sum of existing droplets and CCN can't exceed the background CCN concentrations. As for ice nucleation, Table 1 shows a summary of all the parameterizations used in Bulk. For condensation/deposition freezing, the parameterization of *Cooper* [1986] that was fitted to in situ ice crystal measurements is used. The formulation for immersion freezing used in the scheme is also based on work by *Bigg* [1953], the same as in SBM. The formulation for contact freezing is based on a flux of contact IN to the drops due to Brownian motion, with an effective diffusion coefficient given by *Young* [1974]. Diffusiophoresis and thermophoresis are not considered. The number of contact nuclei is given by *Meyers et al.* [1992]. Droplets are assumed to freeze instantaneously when $T \leq -40$°C. The limit on the maximum cloud ice concentration of 10 cm^{-3} is applied in the scheme, to prevent very large ice number due to homogeneous freezing of cloud droplets. Autoconversion of cloud droplets to raindrops and accretion (collection of cloud droplets by rain) in Bulk follow the formula of *Khairoutdinov and Kogan* [2000]. Basically, the number of converted droplets is proportional to $(N_c)^{-1.79}$, where N_c is droplet number concentration. However, *Khairoutdinov and Kogan* [2000] do not consider self-collection of raindrops as in work by *Seifert and Beheng* [2001] and other schemes.

Table 1. The Droplet and Ice Nucleation Parameterizations Used in SBM and Bulk

Microphysical Processes	SBM	Bulk
Droplet activation	Based on Köhler theory [*Khain et al.*, 2004]	Empirical eqn. following *Twomey* [1959]
Condensation/deposition freezing	*Meyers et al.* [1992]	*Cooper* [1986]
Immersion freezing	*Bigg* [1953]	*Bigg* [1953]
Contact freezing	No	*Young* [1974], *Meyers et al.* [1992].
Droplet homogeneous freezing	*Bigg* [1953]	Assuming instantaneous freezing for all droplets when $T \leq -40°C$

Thus, the bulk scheme uses the parameterization of *Beheng* [1994] for self-collection of raindrops, which is similar to the formula of *Seifert and Beheng* [2001]. Autoconversion of cloud ice to snow is parameterized in terms of the vapor diffusion growth rate [*Harringon et al.*, 1995]. Saturation adjustment treatment is used for the diffusion growth of droplets. The scheme predicts mixing ratios and number concentrations of five hydrometeors: cloud droplet, ice, rain, snow, and graupel. More details about this scheme is provided by *Morrison et al.* [2005].

[14] Note that the scheme we use here is different from the version in the standard released WRF model in which droplet number concentration is a fixed number. In this study of aerosol effects, droplet number concentration is included as a prognostic variable based on work by *Solomon et al.* [2009]. In addition, the subgrid vertical velocity used in the droplet nucleation parameterization is coupled to the eddy diffusion coefficient calculated by the Yonsei University (YSU) planetary boundary layer (PBL) scheme following *Morrison et al.* [2005], to provide more realistic simulation of droplet number concentration for coarse-scale simulations.

3.3. Design of Numerical Experiments

[15] WRF simulations for the two cloud cases have been performed using realistic boundary conditions. Two nested domains with a horizontal resolution of 12 km and 2.4 km are used (Figure 2a) with 51 vertical levels. The numbers of horizontal grid points for Domain 1 (coarse-grid domain) and Domain 2 (fine-grid domain) are 110×90 and 251×201, respectively. The 6-hourly NCEP FNL (Final) Operational Global Analysis data on a 1° by 1° grid are used to provide initial and boundary conditions for Domain 1. To reduce computational time, we used the "nest down" approach in which simulations for Domain 2 are performed separately with initial and lateral boundary conditions obtained from Domain 1. While runs for Domain 1 were performed using the two-moment bulk scheme, the nest down runs for Domain 2 were performed using both SBM and Bulk for comparison. The boundaries for Domain 2 are initialized with data from Domain 1 every 3 h. With nest down, one-way nesting is used such that only meteorological variables such as water vapor and temperature are passed to the inner domain at the boundaries. The microphysical variables such as cloud water and ice are not passed to the inner domain.

[16] To examine aerosol effects, simulations are run under the present polluted condition and a relatively clean condition roughly corresponding to 30–40 years ago [*Qian et al.*, 2009]. Simulations with the SBM are referred to as "C_sbm" and "P_sbm" for the clean and polluted cases, respectively. Similarly, with the Morrison two-moment bulk scheme, they are referred to as "C_bulk" and "P_bulk," respectively. The Goddard shortwave radiation scheme and RRTM longwave radiation scheme are used in this study. Droplet effective radius used in the Goddard scheme is calculated based on cloud droplet and mass concentrations calculated from microphysics.

[17] The initial CCN distribution in SBM is determined by the power law function as shown in equation (1) using critical supersaturation for each size bin. Parameters c and k for the clean and polluted cases are shown in Table 2. The initial CCN size distributions determined by the parameters for the SBM simulations are shown in Figure 2b. For the polluted condition, the number of CCN of diameter (Dp) > 0.65 μm is similar to the available measurements. The total CCN number concentration in the polluted case (with c of 3000*0.231 and k of 0.308) is about 8600 cm^{-3}, which is close to the aerosol concentrations of about 10^4 cm^{-3} measured in Jinan (a city in central East China) during summer [*Gao et al.*, 2007]. But size distribution chosen is relatively arbitrary since observations are not available. *Qian et al.* [2006] indicated the emissions from fossil fuel consumption increased by about 9 times from the 1950s, and about 6 times from the 1970s compared to the 2000s. Therefore, in our clean case, CCN is prescribed to about 1/6 of the polluted case to mimic the conditions about 30–40 years ago in China before the economic development, since scaling of the emissions may not accurately represents the change of aerosol concentration. Because SBM is not designed for coarse resolution simulations and to ensure that the initial and lateral boundary conditions for Domain 2 are the same for both the SBM and bulk runs, Domain 1 is run with Bulk that includes CCN activation by subgrid vertical velocity, with CCN set differently for the clean and polluted scenarios (Table 2) to provide initial and boundary conditions for the corresponding clean and polluted simulations for Domain 2. As shown in Table 2, the CCN representation in the initial time step is the same in the both bulk and SBM simulations. The difference is that CCN size distribution is prognostic in SBM but CCN are prescribed using fixed constants of c and k in Bulk. To be closer to the setup in Bulk, CCN are also prescribed uniform spatially and vertically in the initial time step in the SBM runs. Although not a focus of this study, the uniform vertical treatment of CCN initially could affect anvil properties, but it should not matter much to convection/precipitation especially when the aerosol direct effect is not considered.

[18] For the DCC case, Domain 2 is initialized at 1200 UTC 16 July, 6 h after Domain 1 is initialized, and run for 36 h. The initial profiles of temperature (T), dew point temperature (T_d), water vapor mixing ratio, U and V wind

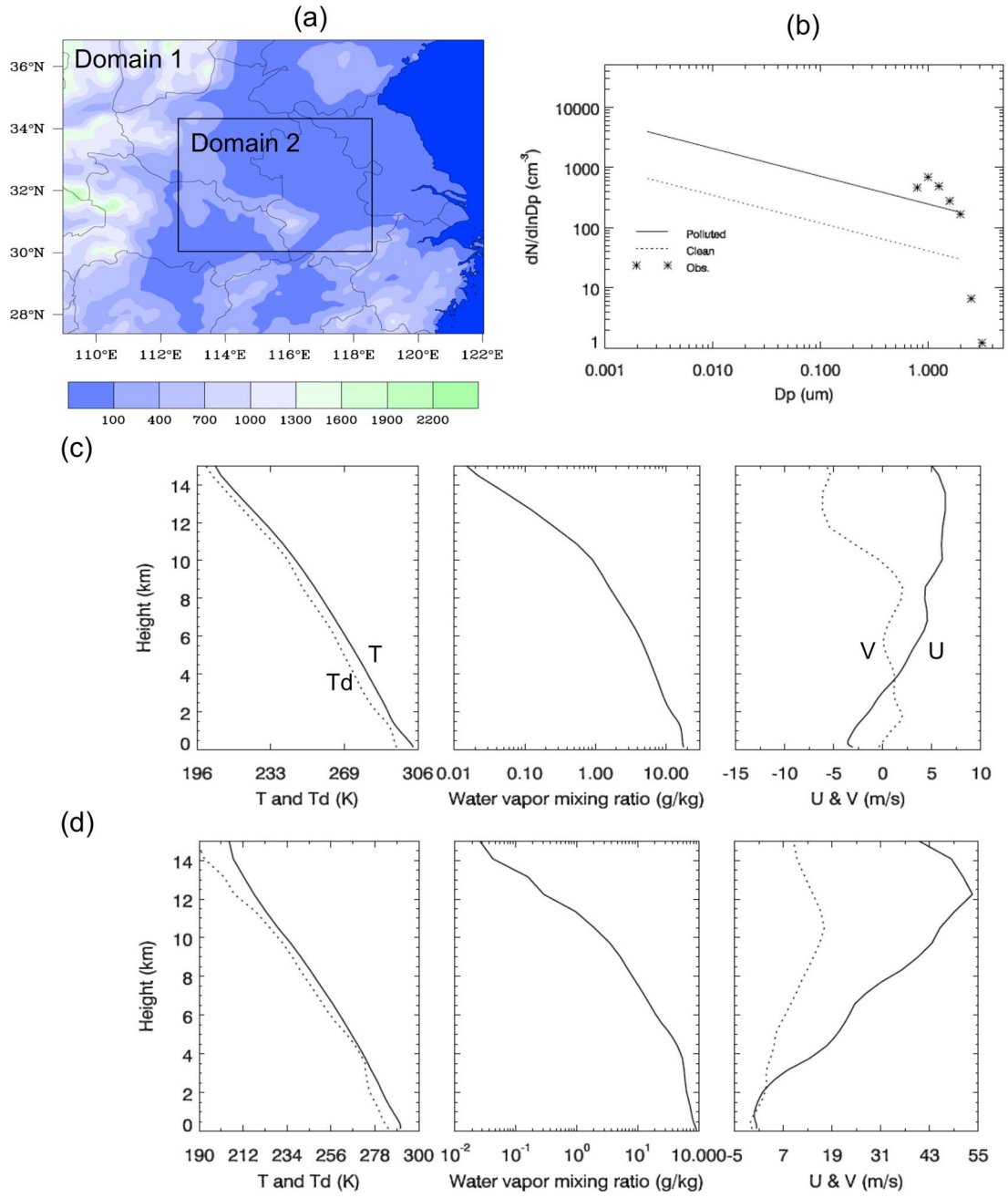

Figure 2. (a) Two nested domains with a horizontal grid-spacing of 12 km and 2.4 km, (b) the initial CCN size distribution for P_SBM and C_SBM, and the initial profiles of T, T_d, water vapor mixing ratio, U and V wind components averaged over Domain 2 for (c) the DCC case and (d) the SC case. The contours in Figure 2a denote the surface elevations and the dark blue denote sea. The star symbol denotes the available measured CCN concentrations at supersaturation of about 0.5% averaged over November 6 and 7.

components are shown in Figure 2c, indicating that the case is humid with weak vertical wind shear. The surface dew point temperature is about 23°C, indicating warm-based clouds. For the SC case, the simulations for Domain 1 start at 1200 UTC 15 November and run for 60 h since the event originated from a cold front that evolved to stratus clouds. Again, simulations start 6 h later for Domain 2. From the initial profiles of T, T_d, water vapor mixing ratio, U and V for Domain 2 runs (Figure 2d), we know that a cloud layer exists around 3.5–4.5 km and the vertical wind shear is extremely strong in the middle and upper troposphere. To avoid artificial removal of aerosols by the incoming air from the lateral boundaries, aerosol sources are set up at the lateral boundaries that include the outer 5 grid cells on each side of

Table 2. The Initial CCN Setup for the Domains Under Clean and Polluted Conditions

	Microphysical Schemes	CCN Setup	
		Clean	Polluted
Domain 1	Bulk	C = 500*0.231 K = 0.308	C = 3000*0.231 K = 0.308
Domain 2	SBM and Bulk	C = 500*0.231 for Bulk[a]; 500 for SBM K = 0.308	C = 3000*0.231 for Bulk; 3000 for SBM K = 0.308

[a]In SBM, C is set to be 500 and 3000 for the clean and polluted cases, respectively. Since the derived size distribution based on these parameters are in natural logarithm in SBM, the total number concentrations integrated over the size distribution should be multiplied by a constant 0.231. Therefore, in the simulations with Bulk, C is multiplied by this constant.

Domain 2. CCN and cloud drop concentration are diagnosed rather than predicted for clouds at the lateral boundaries.

4. Results and Discussions

4.1. The DCC System

4.1.1. Comparison With Observations

[19] First, we evaluate the simulated clouds using available observations from the AMF site at Shouxian. For comparison with the measurements from the single point at Shouxian, the model results are averaged over a volume of 3×3 grid cells (i.e., 7.2×7.2 km^2) near that point. Figure 3 presents the comparisons of liquid water content (LWC) (sum of cloud droplet water and rainwater content), LWP, cloud base and top heights among P_sbm, C_sbm and observations. Since comparisons of the bulk simulations with observations are worse than the SBM runs and do not provide additional information, the bulk simulations are not included in the figure, but will be discussed below. As shown in Figure 3a, the Microwave Radiometer Profiler (MWRP) did not work because of the storm and heavy rain at 18:00–20:00 LST. LWC should peak sometime during this period when the storm cloud occurred. In P_SBM, LWC peaks around 19:00 LST (Figure 3b), meaning the timing of the storm is close to the observations, although the modeled cloud at SX starts a couple of hours earlier. After 20:00 LST,

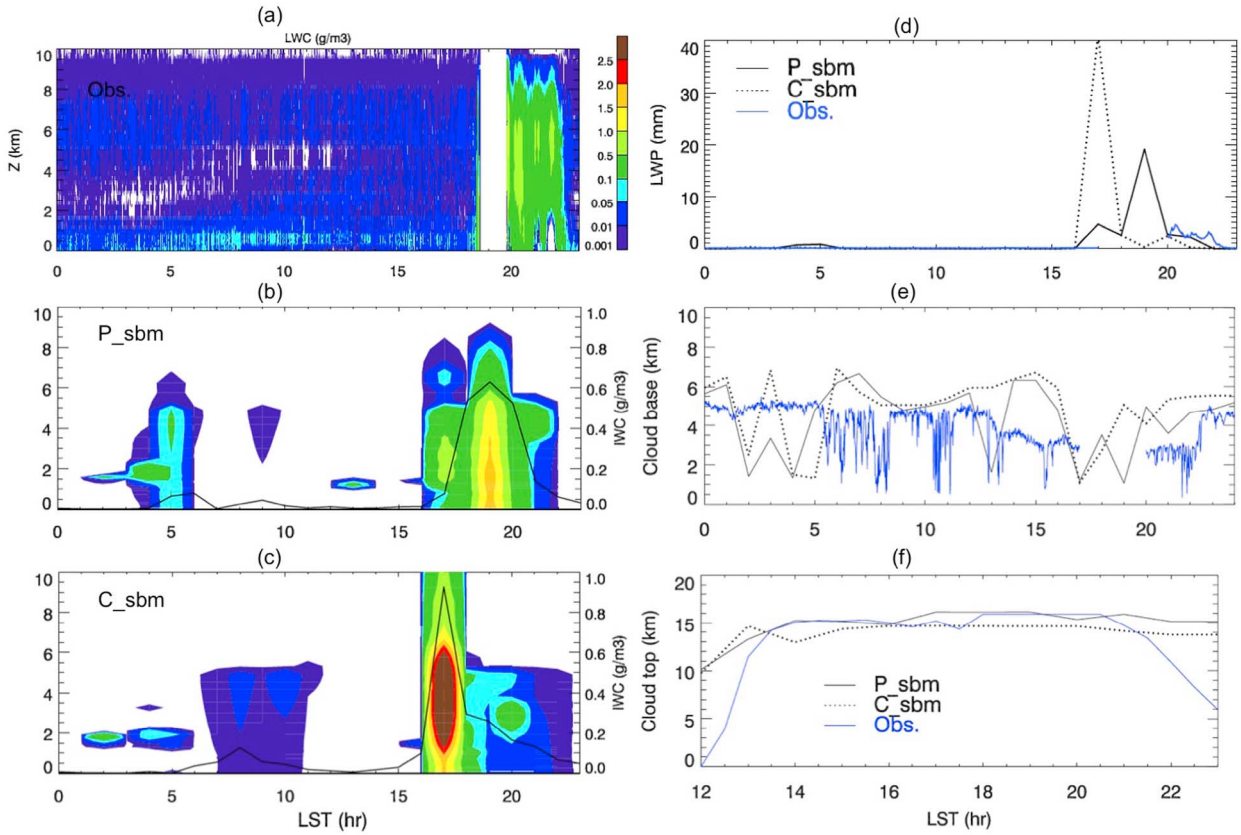

Figure 3. Time series of LWC (g cm^{-3}) profile retrieved from (a) MWRP at SX, (b) P_sbm and (c) C_sbm. The comparison of the times series of (d) LWP (mm) and (e) cloud base height (km) retrieved from MWRP and (f) cloud top height (km) from FY-2 satellite with the modeled values from P_sbm and C_sbm for July 17 (LST). The black line in Figures 3b and 3c is the IWC from the corresponding simulation. The model results are averages over a cloud volume of 3×3 grid cells.

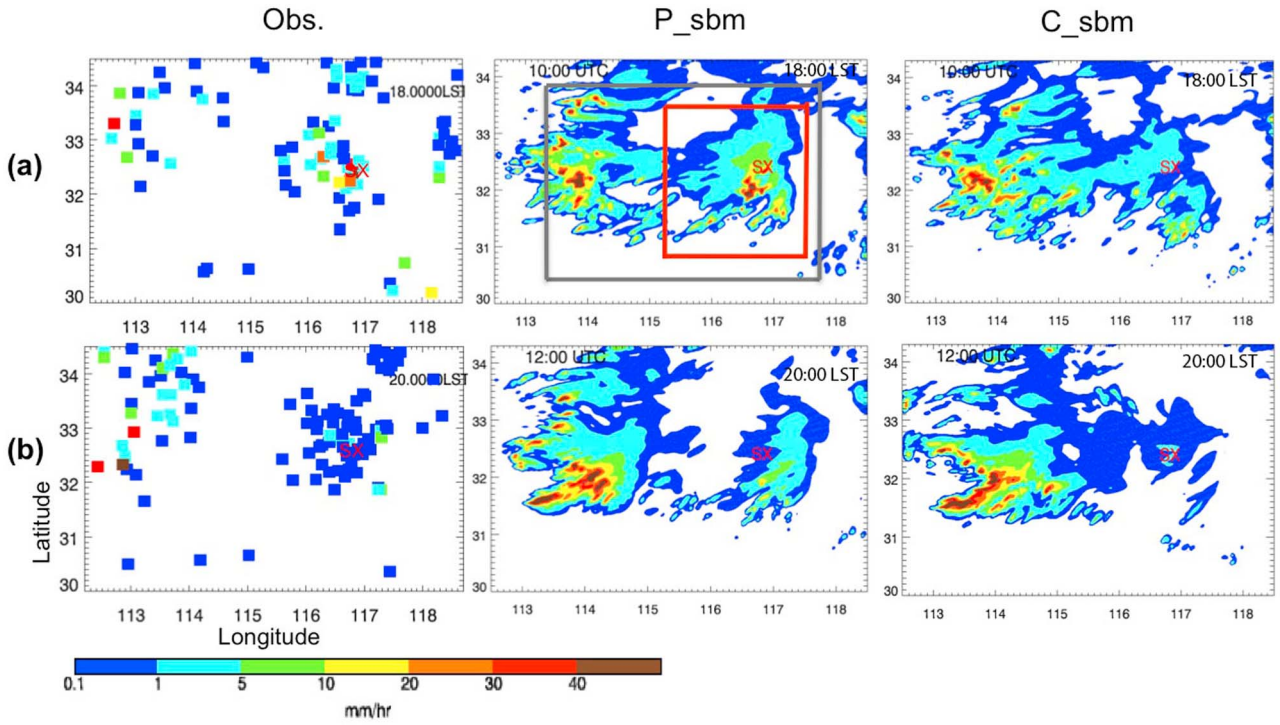

Figure 4. Spatial distribution of hourly rain rates (mm hr^{-1}) from observations, P_sbm and C_sbm at (a) 18:00 and (b) 20:00 LST, which are 10:00 and 12:00 UTC, respectively. Note LST = UTC + 8:00. The red box shows the study region and the gray one denotes the large region for the statistical data in Table 2.

the modeled LWC from P_sbm has a similar magnitude as the observations. However, in C_sbm, LWC peaks at 17:00 LST, about 2-h earlier (Figure 3c) and much higher than P_sbm. The cloud at 5 h in P_sbm was not detected by MWRP, which could be because MWRP only sees clouds directly above the instrument, but the results from the simulations are averaged over a volume of 9 grid cells, of which only 4 grids have clouds at that time. LWC drops off much more quickly relative to P_sbm afterwards and becomes 5–10 times lower than observations after 20:00 LST. The LWC and IWC in P_sbm (Figures 3b and 3c) are lower because the convection cell is much weaker relative to C_sbm at that location. Although we see that the increase in CCN weakens the storm at this location, storms in other places could become stronger (results over a larger region are discussed later). Clearly, the increase in CCN delays the storm by about 2 h. Note that uncertainty of LWC from MWRP is about 30% for these fairly thick clouds. For the SC case where cloud is thinner, the uncertainty can be as high as 60%.

[20] The liquid water path (LWP) in P_sbm agrees with the observations in magnitude very well after 20:00 LST (the values are not shown for 18–20:00 LST) (Figure 3d). The uncertainty of LWP from the MWRP is about 30 g m^{-2} (about 0.03 mm), which is small relative to the high LWP in this case. Obviously, C_sbm predicts a few times larger LWP and the timing is much earlier. The modeled cloud base heights from P_sbm are generally larger than the observed values from MWRP, which has an uncertainty of about 0.5 km (Figure 3e), and the simulated cloud top height of about 15 km is in good agreement with the Chinese Feng-Yun-2 (FY-2) geostationary meteorological satellite measurements (Figure 3f). The model, however, does not capture the decrease of cloud top height after 21:00 LST, suggesting a slower dissipation of cloud anvils in the model, which could be related to the enhanced anvil formation due to the uniform vertical distribution of CCN. Generally, somewhat higher cloud base and lower cloud top are seen in C_sbm relative to P_sbm, implying the invigoration effect of CCN on the DCC. Note that the cloud top height is retrieved with the method of SB2 DART 2 (Santa Barbara DISORT Atmospheric Radiative Transfer) [*Zhou et al.*, 2008] from FY-2 and the uncertainty is very difficult to estimate, although it is known that the uncertainty could be very large above 10 km.

[21] The spatially distributed hourly precipitation data (measured by rain gauges) obtained from China Meteorological Administration (CMA) allow us to compare the modeled and observed system more closely. Figure 4 shows the spatial distribution of hourly rain rates from observations, P_sbm and C_sbm at 18:00 (Figure 4a) and 20:00 LST (Figure 4b). Note that most of the blank area in the panels for observations indicates no rain or very light rain (<0.1 mm hr^{-1}) rather than lack of data as the spatial distribution of the meteorological stations is dense. Overall, the model tends to predict a strong convective system and overestimate rain rates. Since the distribution of rain gauges is coarser in the area west of 116 E, the observations may not capture the entire rain system indicated by P_sbm. The rain pattern from P_sbm resembles the observations both spatially and temporally. For example, the precipitation around Shouxian (SX for short) is very strong at 18:00 LST in both P_sbm

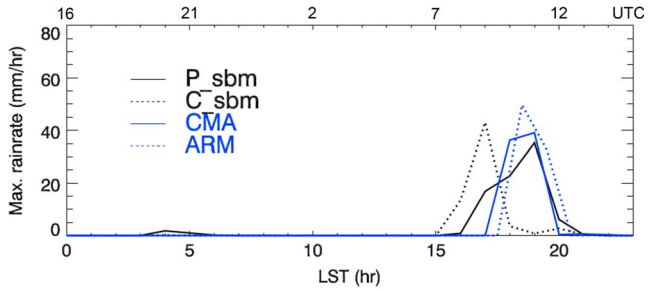

Figure 5. Comparisons of the time series of rain rates (mm hr^{-1}) at Shouxian from the ARM surface meteorological measurement, CMA, P_sbm and C_sbm for July 17 (LST).

and observations (Figure 4a), and becomes much weaker two hours later (Figure 4b). However, in the clean case, strong convection/precipitation is not found around SX at 18:00 LST. In fact, what we see is the dissipating stage of precipitation because the storm occurs about 2 h earlier in C_sbm. In addition, the spatial distribution of rain pattern in C_sbm is quite different from P_sbm and observations: strong precipitation is found around the region of 114.5–116E in C_sbm, which is not seen in P_sbm and observations. Therefore, CCN change the spatial distribution of precipitation quite significantly. When comparing the rain rates at SX from the ARM surface meteorological measurement, CMA, P_sbm, and C_sbm (Figure 5), we see a better agreement between P_sbm and the observations. But the rain rate peaks about 2 h earlier in C_sbm, consistent with the LWC shown in Figure 3. Unfortunately, the single-point measurements at the ARM site for such a short time (24 h) and the much coarser CMA precipitation data prevent us from making meaningful statistical comparison (such as scatter or frequency distribution plots) between model results and observations.

[22] Although the simulation with Bulk in the polluted environment (P_bulk) is also able to simulate the convective system around SX, it predicts stronger convection/precipitation and higher cloud top height (up to 2 km higher), compared to P_sbm and observations (not shown). The timing of the storm around SX in P_bulk does not differ from P_sbm significantly, although rain duration is shorter in P-bulk. Therefore, we do not see significant impact of microphysical parameterizations on the timing of the storm. Under the clean condition, neither Bulk (C_bulk) nor SBM (C_sbm) captures the general spatial distribution of precipitation.

4.1.2. Effects on Convection/Precipitation

[23] To further investigate the differences of the effects between SBM and Bulk and aerosol effects on the convective system over the SX region, a subdomain covering 31.1–33.3 N and 115.5–117.5 E (about 245 × 187 km^2) where the convective system occurred is selected for further study (the red box in Figure 4a; referred to as "the study region"). Here, to examine the time evolution of the convection system, we confine our analysis to a relatively isolated storm with local dynamics-microphysics feedbacks rather than multiple convective systems with potential large-scale feedbacks for easier interpretation of the modeled results. This way our analysis focuses on the effects of aerosols at the cloud scale rather than large-scale features, which is consistent with our experimental design in which the same boundary conditions from the coarse domain are used in all of the simulations in the fine domain. Nevertheless, we also perform a statistical analysis over a larger area (about 375 × 365 km^2) where multiple convection systems are included (the gray box in Figure 4a; referred to as "the large region") and the results will be discussed.

[24] Figure 6a shows the rain occurrence frequency for different rain rate categories in the study region. Following the World Meteorological Organization (WMO) definition of rain category, light rain is defined as rain rate less than 0.1 mm hr^{-1} and heavy rain is for rain rate larger than 5 mm hr^{-1}. Between 0.1–5 mm hr^{-1}, we divide the rain rate into two intermediate rain categories between 0.1–1 and 1–5 mm hr^{-1}. Both SBM and Bulk consistently show that the increase of CCN reduces the rain occurrence frequency and amount (Figures 6a and 6b) for light and intermediate rain. However, for heavy rain, SBM simulates an increase in rain frequency and amount by over 20% from the clean to polluted condition, but no significant change (i.e., only a few percent decrease) is simulated by Bulk. To determine if the results are robust since the simulation of DCC could be sensitive to initial conditions, we performed 5 ensemble runs for the bulk simulations under each CCN condition by adding random perturbations to the initial temperature over the entire 3D fine domain. The random perturbation is represented by a normal distribution with mean 0 and a standard deviation varying from 0.2 to 0.5 K for different runs. As shown in Figure 6 (blue color), the averaged results from the ensemble runs tell the same story: with bulk, increasing CCN decreases the frequency and amount for light and intermediate rain but no significant change for heavy rain. Although we did not perform similar ensemble runs with SBM because of computational cost, it should be noted that the reduced frequency and amount for light rain and vice versa for heavy rain in the polluted case simulated by SBM are also found in analyses of long-term observational data [*Qian et al.*, 2009; *Yao et al.*, 2008]. Furthermore, invigoration of convection/precipitation by CCN for this case is supported by the finding of *Fan et al.* [2009b], since the observed wind shears are weak with a maximum value less than 8 m s^{-1} within 0–10 km (Figure 2c).

[25] The significant increase in the frequency and amount of heavy rain in the polluted case with SBM suggests the invigoration effect of CCN on deep convection. By examining the profiles of updraft velocity over the study region (Figure 7), the convective strength is indeed stronger in P_sbm compared to C_sbm between 15 and 20:00 LST when the convective system around SX is active. The average w with $w > 2$ m s^{-1} over the study region during 12–23:00 LST is 4.1 m s^{-1}, about 5% larger relative to C_sbm. The stronger convection in P_sbm results in ~18% increase in the accumulated surface precipitation relative to C_sbm (Figure 6c). However, with Bulk, the clean case (C_bulk) predicts stronger convection than the polluted case (P_bulk) with an increase of maximum updraft velocity from 36.2 m s^{-1} in P_bulk to 43.6 in C_bulk over the study region. Overall, convection is suppressed, rain rate is decreased, and the accumulated surface precipitation is reduced by increasing CCN with the bulk scheme. From

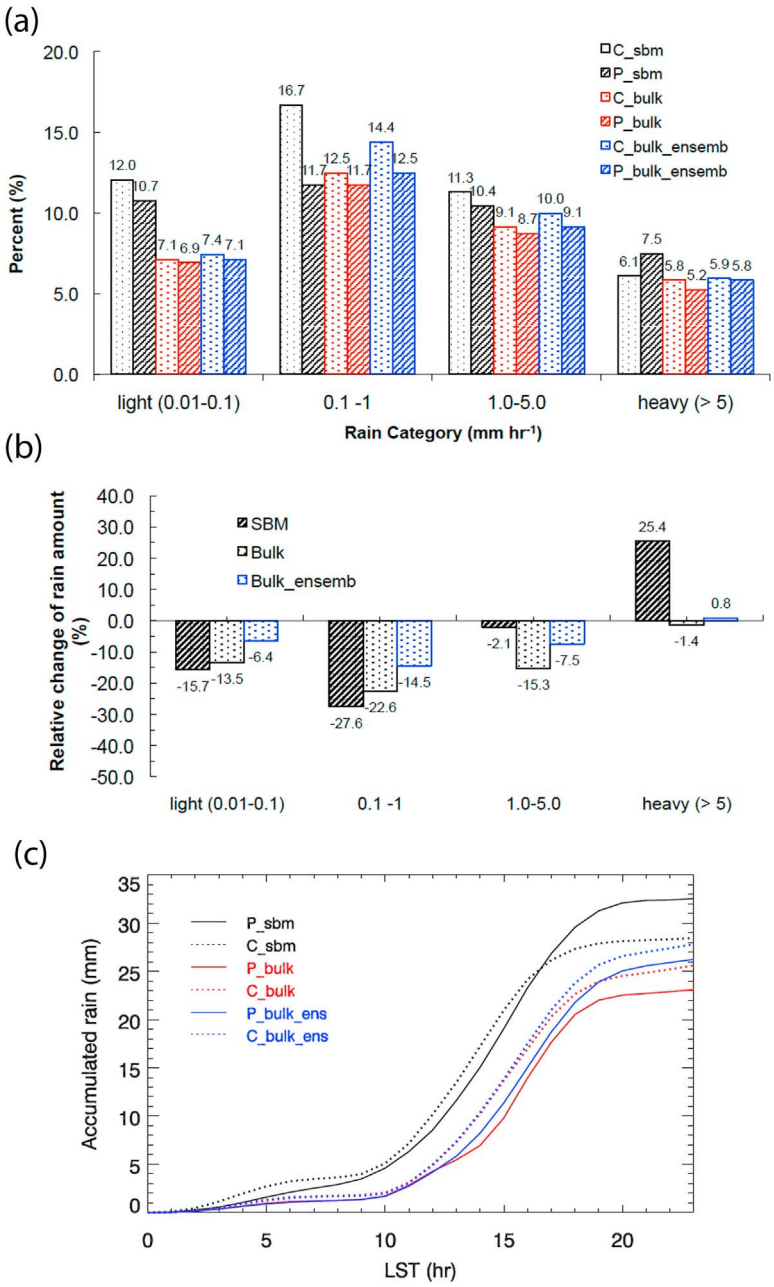

Figure 6. (a) Percentage of rain occurrence for each rain category in the study region for July 17 (0–23:00 LST), (b) relative change of rain amount from clean to polluted condition simulated by SBM and Bulk for each rain category, and (c) accumulated precipitation on the surface averaged over the study region. The rain occurrence frequency is calculated by the number of grid points falling in a certain rain category divided by the total grid points during the entire day of July 17. "Ensemb" in the legends represents the ensemble runs shown in blue colors.

Figure 6c, suppression of precipitation by CCN in the beginning of the storm and then invigoration of precipitation later is clearly simulated by SBM. With Bulk, precipitation is reduced by CCN in the afternoon, corresponding to the suppressed convection. Note that P_bulk appears to give stronger convection between 2 and 9 LST than C_bulk, under the conditions of much less activated CCN relative to the afternoon. The ensemble runs with Bulk give similar results in precipitation (Figure 6c, blue line) and convection with the average w of 4.4 in P_bulk over the study region from 12:00–23:00 LST but 4.6 in C_bulk. Although the ensemble average results show a smaller change in the total precipitation and convection from increasing CCN compared to the single simulation results, they are qualitatively consistent.

[26] From Figure 7, we can also see that Bulk generally predicts stronger convection than SBM, a typical feature of many bulk schemes indicated in many past studies [e.g.,

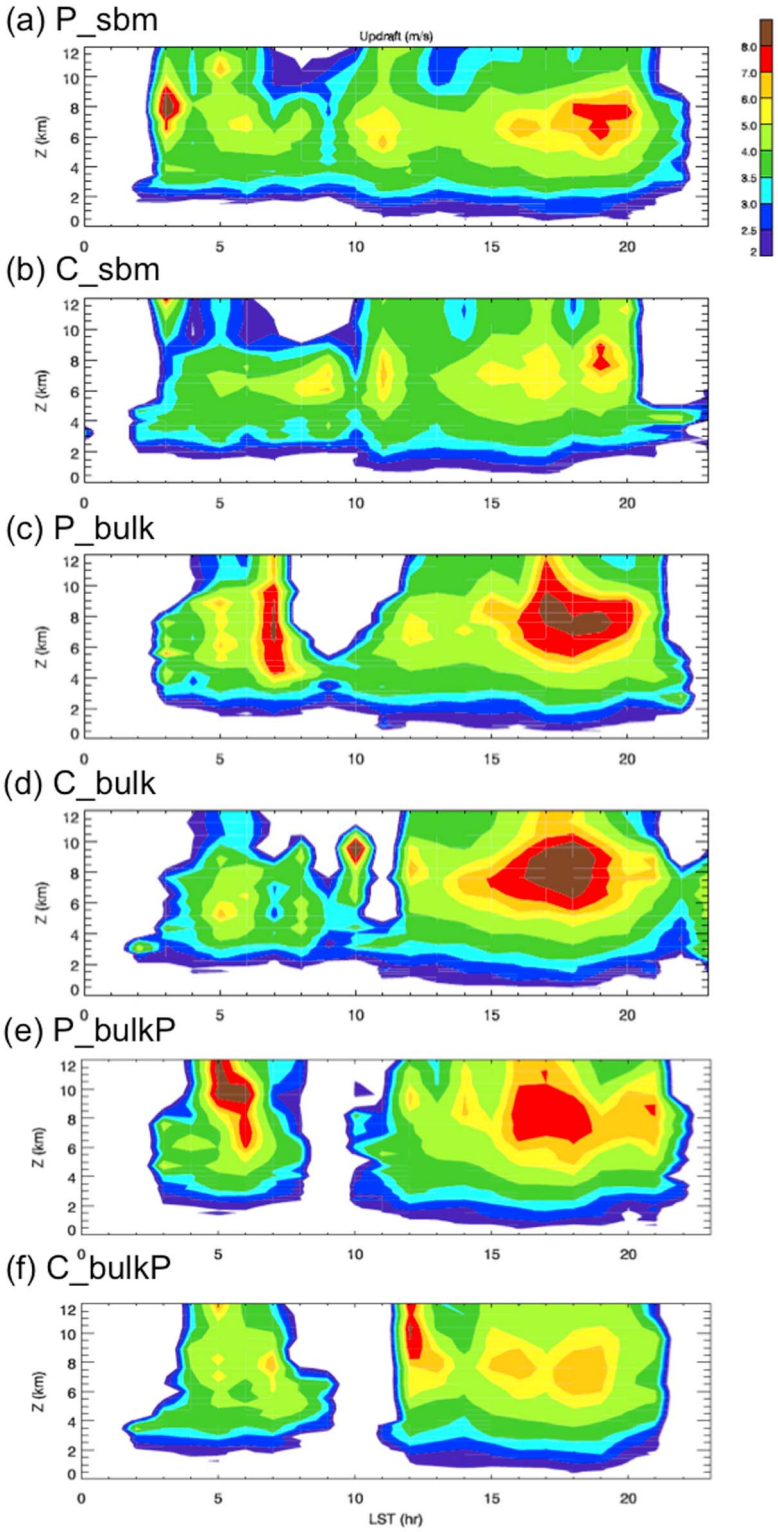

Figure 7. Profiles of updraft velocity (w) (m s^{-1}) from (a) P_sbm, (b) C_sbm, (c) P_bulk, (d) C_bulk, (e) P_bulkP and (f) C_bulkP for July 17 (LST), calculated by averaging over the grids with $w > 2$ m s^{-1}.

Khain and Lynn, 2009; *Tao et al.*, 2007; *Li et al.*, 2009], explaining the higher cloud top heights in P_bulk than P_sbm as shown in Figure 3. The maximum vertical velocity in C_bulk is 43.6 m s^{-1}, while it is only 30 m s^{-1} in C_sbm. The reasons for the stronger convection predicted by bulk schemes with saturation adjustment have been detailed by *Khain and Lynn* [2009]. They suggested that the saturation adjustment method in those bulk schemes cannot accurately

account for the decrease of supersaturation due to droplet growth during a single time step and supersaturation is removed by condensation growth at each time step, leading to overestimation of latent heat release by condensation [*Khain et al.*, 2000, 2008]. Although Bulk predicts stronger convection than SBM, it estimates less accumulated rain, especially in the polluted case, as a result of very different microphysical properties that will be discussed in the next section. Therefore, the differences in convection and accumulated precipitation simulated by Bulk versus SBM are even larger than the aerosol effects on them (Figures 6c and 7). To improve estimates of aerosol indirect effects, it is crucial to further constrain cloud microphysical schemes to reduce model uncertainties.

[27] Averaged over the large region (again, the gray box in Figure 4a), the results in Figure 6 are qualitatively similar to the results averaged over the study region. The relative differences between SBM and Bulk become smaller, which is expected for a larger domain more affected by the same boundary conditions. The aerosol effects on precipitation and updraft velocity for the large region as shown in Table 3a also agree with what we see for the smaller study region, but with much smaller magnitude because they are mainly forced by the domain average convergence from the boundary conditions that are the same in all simulations. Precipitation and updraft velocity listed in Table 3a from the ensemble runs indicate that the results discussed above are robust qualitatively.

4.1.3. Effects on Cloud Microphysical Properties

[28] The different behaviors between SBM and Bulk in the CCN effects on convection and precipitation should stem from very different cloud microphysical properties. Figure 8 shows the averaged hydrometeor number and mass concentrations over the study region. The most striking difference between SBM and Bulk is found in the simulated droplet and raindrop number concentrations. In the polluted case, Bulk (P_bulk) predicts over two times higher droplet concentrations (N_c) and up to 100% higher raindrop concentrations (N_r) relative to SBM during the active convection period, although the differences are small at other times, indicating that the stronger convection predicted by Bulk is one of the factors leading to the stronger droplet nucleation. Another important factor lies in the fixed CCN prescribed everywhere at each time step with Bulk. To figure out how much the fixed CCN contributes to the much higher N_c, we conducted sensitivity tests by fixing CCN size distribution during the simulations with SBM, although an advantage of SBM is in its ability to simulate time-varying CCN size distribution. In these sensitivity runs, N_c is even higher than that simulated by Bulk when CCN is fixed in SBM under both polluted and clean conditions, indicating that the fixed CCN is the major contributor to the high droplet concentration in Bulk. The lower N_c with Bulk than SBM when CCN is fixed is because strong in-cloud scavenging is taken into account indirectly in Bulk (i.e., the total droplet number concentrations in the previous time step is deducted from the newly formed activated droplets).

[29] To further strengthen that the fixed CCN leads to high N_c in Bulk, we have modified the bulk scheme by implementing a prognostic CCN approach in which CCN number and mass are predicted. We conducted tests with this scheme for the clean and polluted cases (referred to as "P_bulkP" and "C_bulkP," respectively; blue color in Figure 8). Clearly, the prognostic CCN approach gives much closer N_c compared to that of SBM. However, N_r is much higher than the simulation with the fixed CCN because the autoconversion rate becomes about 2 times higher due to larger droplet size resulted from lower N_c (N_r will be discussed more in the following paragraph). This further indicates that the fixed CCN is responsible for the much higher N_c predicted by Bulk relative to SBM. Note that the results for the prognostic CCN approach in Bulk are preliminary, so we only show the results for liquid particles to support our argument that the fixed CCN leads to much higher N_c. We will present more in-depth analysis of the prognostic CCN scheme in a follow-on paper.

[30] We performed additional simulations with Bulk and found that the subgrid droplet nucleation considered in Bulk through subgrid vertical velocity exerts little effect on the clouds (although it probably will have more impact in simulations with much coarser resolutions).

[31] The higher N_r in Bulk relative to SBM is significantly contributed by the much smaller cutoff size between droplets and raindrop in Bulk (25 μm versus 100 μm in SBM). Sensitivity test based on P_sbm in which only the cutoff size is modified to be $\sim$25 μm shows that N_r averaged over the study region in July 17 is increased from 0.09 to 0.145 L^{-1}, much closer to 0.13 L^{-1} in P_bulk. N_c does not change significantly by the cutoff size. Note that the actual simulations with SBM do not depend on the cut-off size since the cutoff size is only used for outputting diagnostic quantities Q_c/Q_r and N_c/N_r. N_r in Bulk is also strongly affected by the assumed size for the newly formed raindrops. When the assumed radius increases from 25 to 40 μm which is used by *Seifert and Beheng* [2001] and *Li et al.*, [2008], N_r is decreased by about 6 times. In addition, parameterizations of self-collection of raindrops and rain evaporation below cloud base could also affect N_r [*Seifert*, 2008].

[32] Under the polluted condition, Bulk predicts up to 4 times higher N_c and up to 2 times higher N_r than SBM (Figure 8). However, the differences in droplet mass (Q_c) and raindrop mass (Q_r) concentrations between P_sbm to P_bulk are not as large as their number concentrations. This implies that the mean droplet and raindrop sizes in P_sbm are larger than those of P_bulk. Indeed, the mean droplet radius in P_sbm is about 45 μm, while it is only about 5 μm in P_bulk. For raindrops, the mean radius is about 350 μm in P_sbm, only about 15% larger than that in P_bulk. Besides the much lower N_c, the much larger cutoff size to distinguish cloud droplets and raindrops in SBM also contribute substantially to the larger cloud droplet size relative to P_bulk. The mean radius is reduced to 12 and 330 μm for droplets and raindrops, respectively, when the cutoff size is assumed to be $\sim$40 μm.

[33] To explain why the strong droplet nucleation leads to the suppressed convection in the polluted case with Bulk, we examined the time series of vertical profile of IWC and N_i in both P_bulk and C_bulk. It is found that IWC is lower in P_bulk but N_i has little differences at $-15 < T < -30$°C over the active convection period compared with C_bulk. The reduced ice mass in P_bulk could be attributed to deposition and droplet freezing because of the much smaller

Table 3a. Quantities Averaged Over the Large Region (30.5°N–33.8°N and 113.5°E–117.5°E), i.e., 3-D Domain Average, for DCC in July 17 (LST)

	P_sbm	C_sbm	P_bulk	C_bulk	P_bulk_ensemb	C_bulk_ensemb	Changes With SBM[a] (%)	Changes With Bulk (%)	Changes With Bulk Ensemble (%)
N_c (cm^{-3})	5.43	1.06	10.86	2.39	11.09	3.86	414	355	187
N_r (L^{-1})	0.125	0.222	0.140	0.367	0.145	0.335	−43.7	−61.9	−56.7
N_i (L^{-1})	25.5	20.3	28.1	27.2	26.5	28.5	25.6	3.2	−7.02
N_g (L^{-1})	0.097	0.330	0.175	0.179	0.280	0.190	−70.6	−2.2	47.4
Q_c (g kg^{-1})	0.012	0.01	0.008	0.007	0.008	0.00755	20.0	14.3	5.96
Q_r (g kg^{-1})	0.044	0.045	0.038	0.041	0.04	0.042	−2.22	−7.32	−4.76
Q_i (g kg^{-1})	0.069	0.058	0.043	0.044	0.037	0.045	19.0	−2.27	−17.8
Q_g (g kg^{-1})	0.012	0.021	0.0335	0.0331	0.031	0.036	−42.86	1.2	−13.9
w[b] (>2 m s^{-1})	3.93	3.81	4.22	4.33	5.31	5.40	3.15	−1.9	−1.11
Rain[c] (mm)	11.47	11.03	8.33	8.71	8.32	8.67	3.99	−4.36	−4.04

[a]The changes are calculated by (P_sbm-C_sbm)/C_sbm*100%.
[b]Here w is averaged over the time from 12:00 to 23:00 in July 17, when the major convective systems occur.
[c]Precipitation is the accumulated rain in that day averaged over the large region.

droplet sizes. Since latent heat of freezing is proportional to the produced ice mass, it suggests that latent heat release is reduced in P_bulk relative to C_bulk, explaining the suppressed convection by CCN with Bulk. It should be noted that, in the modified Bulk with the prognostic CCN, the invigoration effect on convection and the enhanced heavy rain in the polluted case occurs: from C_bulkP to P_bulkP, the averaged w over grid points with w > 2 m s^{-1} between 12 and 23:00 LST is increased from 4.1 to 4.4 m s^{-1}m, and the heavy rain frequency and amount is increased by 4% and 7% respectively. These results are consistent with SBM. Similarly, the CCN invigoration effect does not occur with SBM when CCN is fixed, because unrealistically strong droplet nucleation makes N_c too high and droplet freezing becomes very inefficient in the polluted case (far beyond optimal for invigoration effect). All these tests consistently

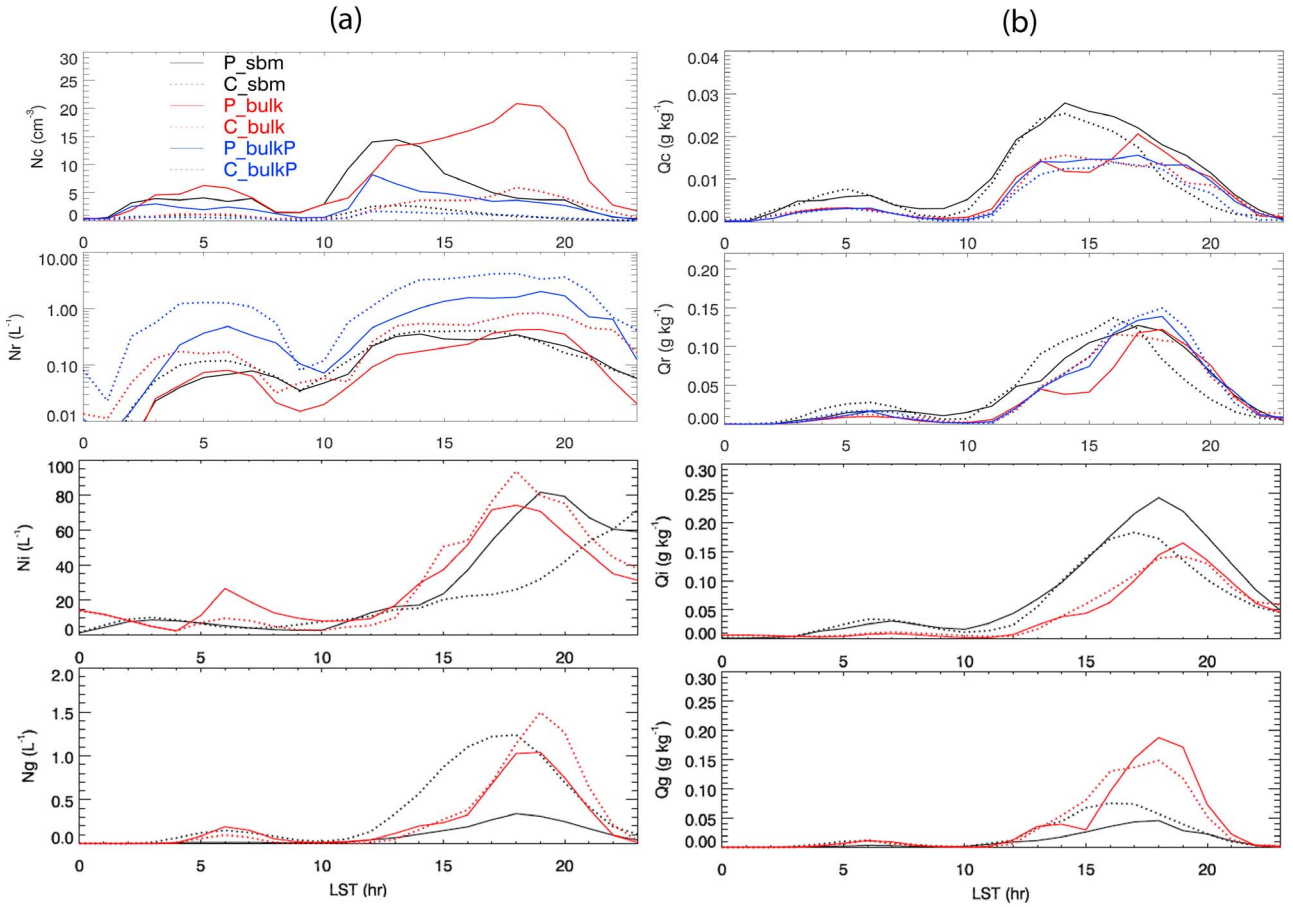

Figure 8. Time series of domain-averaged (a) number and (b) mass concentrations for cloud droplet, raindrop, ice/snow, and graupel/hail over the study region.

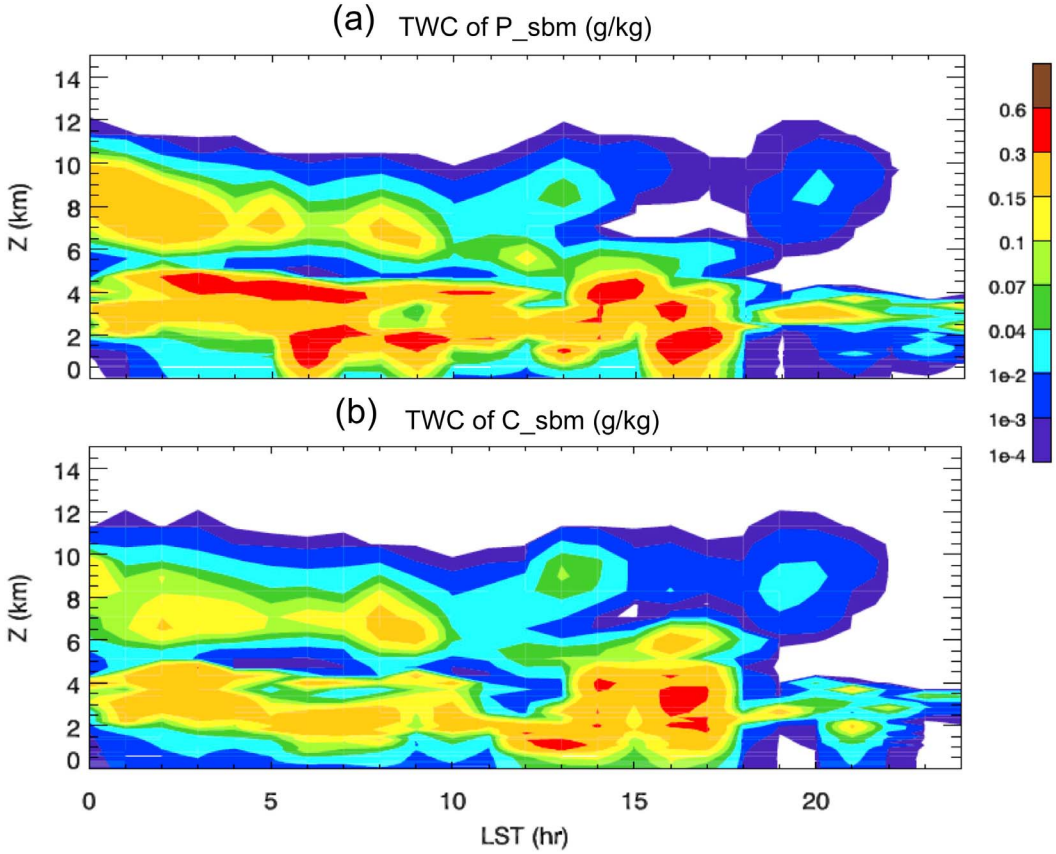

Figure 9. Time series of TWC (g cm^{-3}) around Shouxian from (a) P_sbm and (b) C_sbm in Nov 07.

indicate that unrealistically strong droplet nucleation due to the fixed CCN is primarily responsible for suppressed convection simulated by the original bulk scheme.

[34] Under the clean condition, differences in N_c and N_r between SBM and Bulk are even larger (Figure 8). As discussed above, the reasons could be attributed to (1) the much larger cutoff size in SBM than Bulk in distinguishing droplets from raindrops and (2) the different conversion rates from droplets to raindrops between SBM and Bulk. By examining the differences of Q_c and Q_r between C_bulk and C_sbm, we find that the mean droplet and raindrop sizes in C_sbm are larger than those of C_bulk, but with the differences much smaller than those under the polluted condition. In any case, Bulk generally predicts much higher N_c and N_r but smaller droplet and raindrop sizes compared to SBM. These differences are related to the stronger nucleation and smaller cutoff size between droplet and raindrop discussed in the previous paragraph, explaining the lower surface precipitation rate (small drops sediment slowly and may evaporate completely before reaching ground).

[35] An increase in CCN significantly increases N_c and Q_c but decreases N_r; SBM and Bulk qualitatively agree with each other on this point. Increasing CCN significantly increases N_i (sum of ice and snow number concentrations) with SBM, but with Bulk a decrease of N_i is seen after 14 LST in Figure 8. Averaging over the large region, there is a slight increase (3.2%) in N_i by increasing CCN (Table 3a), but the increase is much smaller than those of SBM and other studies that used bulk schemes [*Wang*, 2005; *Li et al.*, 2008]. This can be explained by the suppressed convection by CCN with Bulk and a limit on the maximum cloud ice concentration of 10 cm^{-3} applied to the Morrison scheme. N_i often exceeds 10 cm^{-3} in both P_sbm and C_sbm since in SBM only a limit of supersaturation over ice no larger than 50% is used for condensational/depositional freezing. Currently it is uncertain how high the maximum ice number can be. Since convection is enhanced by increasing CCN with SBM, and the Meyer's parameterization employed in SBM tends to predict a very high ice formation rate at high supersaturation, it is not surprising that N_i is increased in the polluted case with SBM.

[36] Both SBM and Bulk predict a decrease of N_g (sum of graupel and hail number concentrations) in the polluted condition. However, they do not agree on the CCN effect on Q_i (sum of ice and snow mass concentrations) and Q_g (sum of graupel and hail mass concentrations). SBM predicts up to 35% higher Q_i in the polluted case (19% on average in July 17 over the large region as shown in Table 3a), but no significant change is seen from C_bulk to P_bulk. With SBM, Q_g is decreased by increasing CCN, but there is no significant change with Bulk statistically (Table 3a). The decreased N_g by the increase of CCN with SBM is because riming efficiency is reduced due to the reduced droplet and ice particle sizes. With Bulk, the reduced N_g in the polluted case is related to the decreased raindrop mass and number. Therefore, with Bulk, the much lower N_g and not much change in Q_g in the polluted case suggest larger graupel/hail sizes relative to the clean case. This is likely related to the

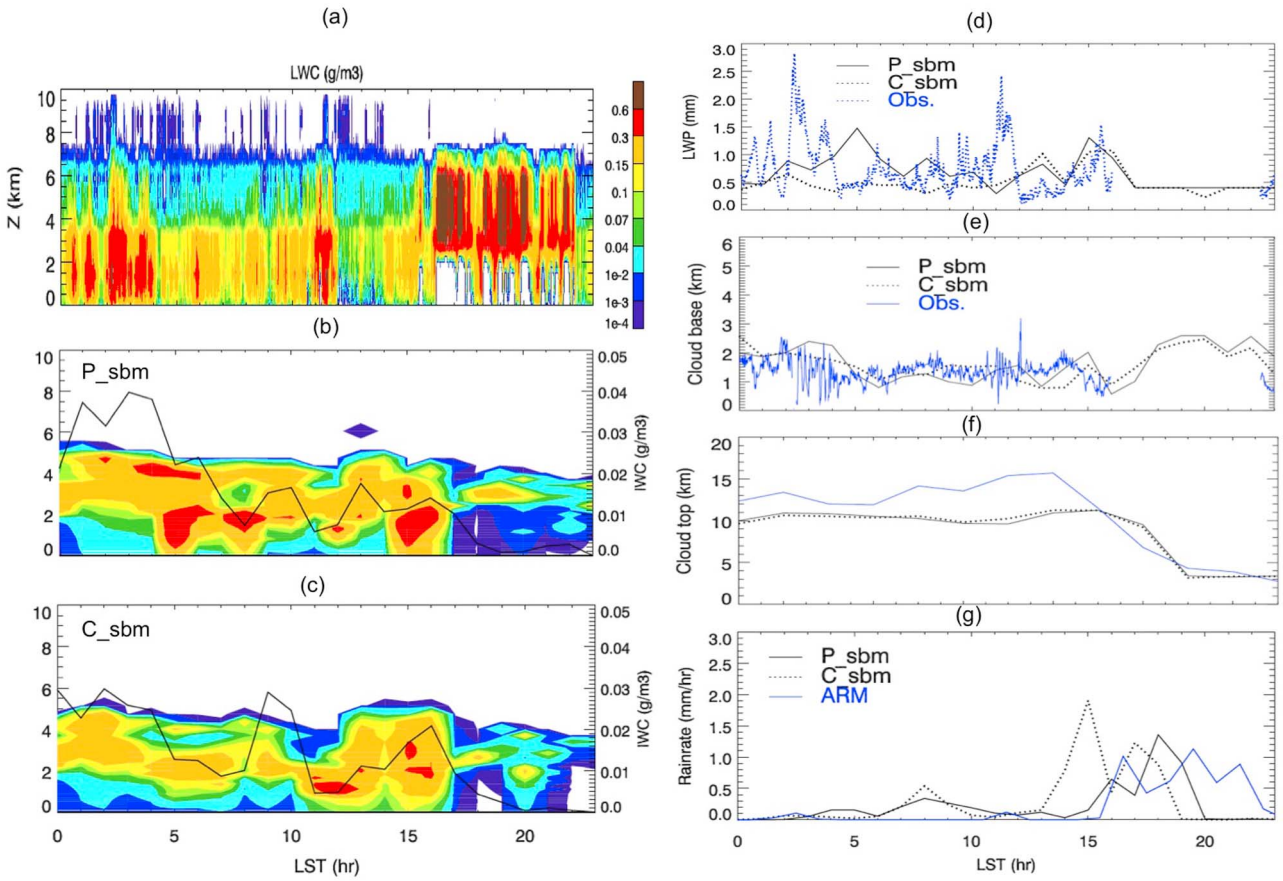

Figure 10. (a–f) Same as Figure 3 but for Nov 07 (LST). (g) Comparisons of the time series of rain rates (mm hr^{-1}) at Shouxian from among P_sbm, C_sbm and ARM observations.

simple parameterization of the riming process in Bulk in which riming rate is determined by a constant and the constant is uncertain. In fact, riming efficiencies are not only a function of particle size but also a function of ice crystal habit [*Pruppacher and Klett*, 1997], and the SBM representation is also uncertain since our understanding is not sufficient to well represent ice processes. As a result, SBM and Bulk can produce even qualitatively very different results [*Muhlbauer et al.*, 2010]. Figure 8 also shows that, with Bulk, CCN produce significant effects on the properties of liquid particles but not ice particles, while CCN produce significant effects on both liquid and ice microphysical properties with SBM. The significantly increased Q_r and Q_i in the polluted case with SBM explain the enhanced precipitation. However, with bulk, Q_r and Q_i are decreased by the increase of CCN, explaining the decreased accumulated precipitation.

[37] Averaged over the large region, our major results in microphysical properties such as mass and number concentrations of cloud droplet and ice are not changed, except the peaks in the time series plots are less pronounced because multiple convective systems occur at different times and evolve differently. It suffices to note that there are no qualitative changes in the differences of the cloud microphysical properties between SBM and Bulk (Table 3a). As for aerosol effects, the results from the large region agree with those from the study region: from clean to polluted, Nc and Q_c are increased but N_r and N_g are decreased. SBM and Bulk agree with each other on this. Q_r is decreased significantly with Bulk but not with SBM. We also see that SBM predicts much larger change in N_i and Q_i by CCN than Bulk. The ensemble runs for Bulk do not change the conclusions qualitatively, except for graupel (larger CCN effects on N_g and Q_g for the ensemble results; Table 3a), which could be associated with over-simplified parameterization as discussed above.

4.2. The SC System

4.2.1. Comparison With Observations

[38] As shown in Figure 1b for the SC case, the clouds are separated into two layers, with upper ice clouds and lower stratiform clouds. By examining the total condensed water (TWC) around SX from P_sbm (the same grid cells as the previous case), one can see that the simulated clouds from P_sbm capture the two-layer feature very well (Figure 9a). Also, by comparing Figures 9 and 10, we know that the upper layer is composed of mainly ice and the lower layer mainly liquid. Since the clean case (C_sbm) has similar cloud structure as P_sbm (only lower TWC; Figure 9b), CCN do not change the cloud structure for this cloud system because it is mainly controlled by boundary layer mixing and capping inversion. Comparison of the profiles of LWC among P_sbm, C_sbm and observations from MWRP at SX is shown in Figure 10a. After 17:00 LST, the WACR radar

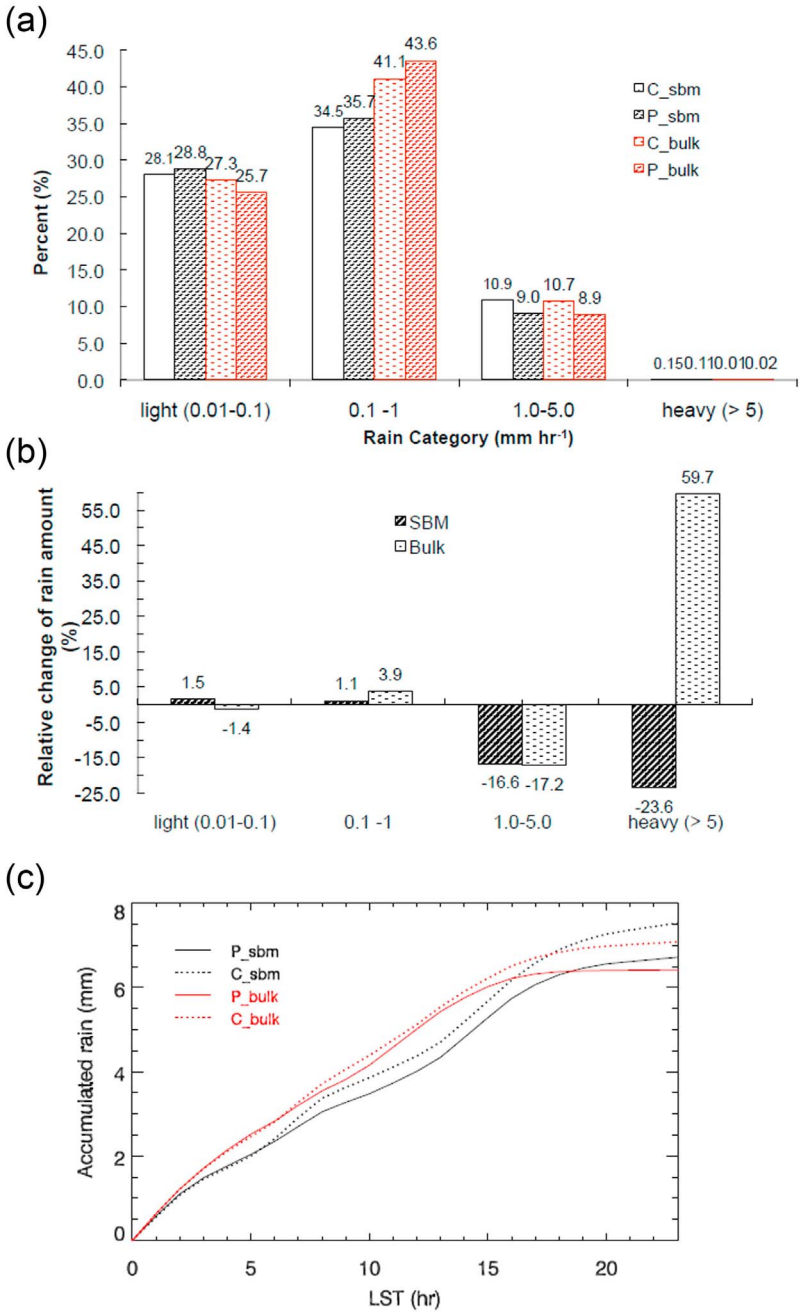

Figure 11. Same as Figure 6 but for Nov 07.

reflectivity only shows a continuous layer of stratus cloud below 4 km but MWRP indicates very high LWC above 4 km. The unusually high LWC signal above 4 km where the cloud radar did not detect anything suggests that the MWRP retrieved data are problematic after 15:30 LST, due to contamination by rain (Figure 10g). Therefore, The MWRP data are removed from the comparisons with the modeled results during 15–22:30 LST. It should also be noted that uncertainty of the retrieved LWC can be as high as 60%, which is not useful to discern which simulation is better in this low LWC case.

[39] LWC from P_sbm is generally consistent with the MWRP data, except for a low bias within the boundary layer and high bias above 4 km. The LWC in the boundary layer for the clean case (C_sbm) is underestimated even more compared to P_sbm. Comparing the two cloud regimes, our modeling results suggest that increasing CCN increases LWC for both DCC and SC. The LWP from P_sbm generally agrees with the observations (Figure 10d). The LWP from the clean case (C_sbm) is smaller, consistent with the lower LWC shown in Figure 10a. As noted in Section 4.1.1, the uncertainty of LWP is low, only about 0.03 mm. The modeled cloud base height in P_sbm agrees well with the observed values from MWRP with an uncertainty of about 0.5 km (Figure 10e), but the modeled cloud top height (Figure 10f) is about 1–2 km lower than the satellite

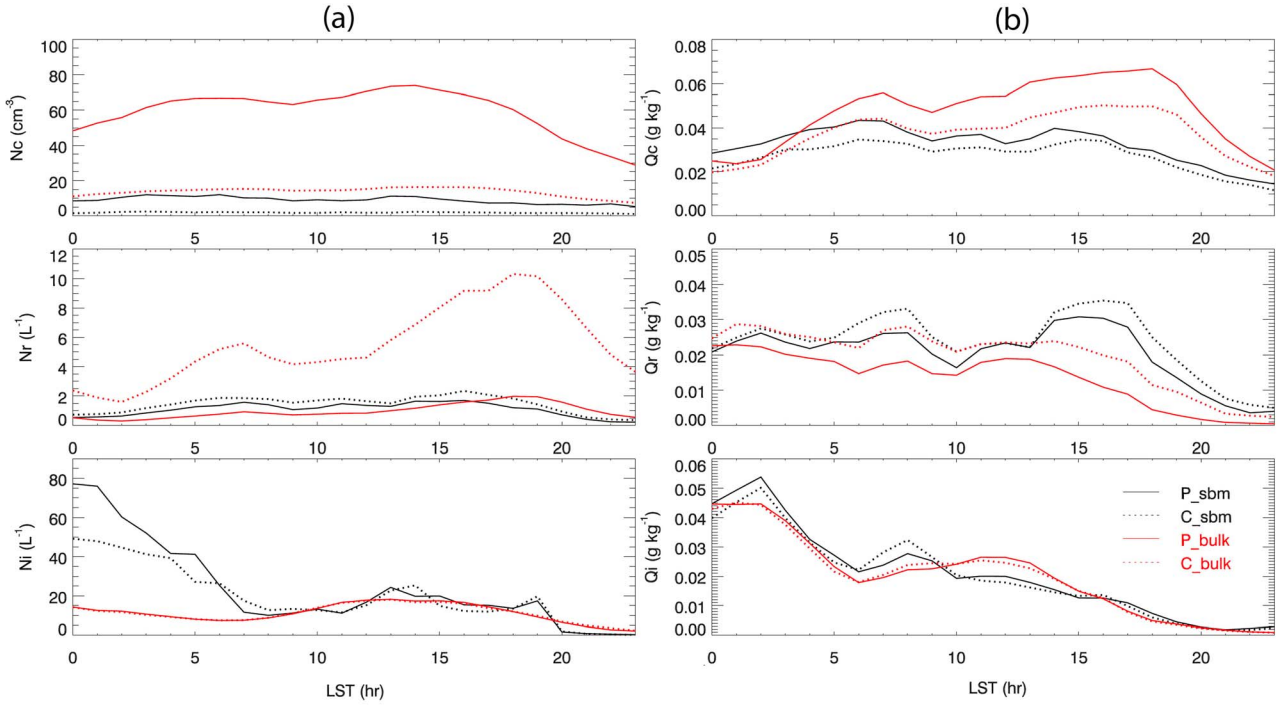

Figure 12. Same as Figure 8 but for Nov 07.

retrieved data from FY-2. However, uncertainty of the retrieved cloud top height could be very large above 10 km and it is known that the retrieved cloud top height is higher than that from the WACR radar (only up to about 10 km from Figure 1b) (M. Cai, personal communication, 2011). One can see that aerosols have little effect on the cloud base and top heights of the SC, which is also different from the previous DCC case.

[40] Time series of precipitation rate from the ARM surface meteorological measurement, P_sbm and C_sbm are shown in Figure 10g. The timing and magnitude for the significant rain event from P_sbm agree well with observations, except that the rain event ends a couple of hours earlier, indicating faster cloud evolution in the model. The peak precipitation in C_sbm is much earlier and also has larger values compared to P_sbm. Therefore, rain is delayed and suppressed by increasing CCN in this case.

[41] Since comparisons of the bulk simulations with observations are not good and do not provide additional information, Bulk results are also not plotted in Figure 10. The simulated SC with Bulk are deeper and there is no clear two-layer feature in either clean or polluted environments. Compared to the corresponding simulations with SBM at the point of Shouxian, Bulk gives lower rain rate, delay of the onset of precipitation, larger LWC and LWP, and higher cloud base and top heights.

4.2.2. Effects on Cloud Microphysical Properties and Precipitation

[42] Similar to the DCC case, aerosol effects are analyzed over the same study region with both SBM and Bulk. The rain occurrence frequency for light rain is not changed significantly by CCN and SBM and Bulk agree with each other (Figure 11a). For intermediate rain, the change of rain frequency by CCN is not significant with both SBM and Bulk, but the rain amount is significantly reduced by 16.6% and 17.2% for SBM and Bulk, respectively. Overall, an increase in CCN does not change rain frequency significantly but reduces the rain amount, and both SBM and Bulk are consistent with each other for the SC (Figures 11a and 11b). Since heavy rain occurs rarely for SC and its contribution to the total rain amount is negligible, we exclude it from the discussion here. For the accumulated rain on Nov 17 averaged over the study region, the reduction by the increase of CCN at 23:00 is about 20% with SBM and 18% with Bulk, and Bulk predicts similar total precipitation as SBM in both clean and polluted conditions (Figure 11c). The significant reduction in total precipitation by the increase of CCN in this SC is not due to the change in convection but rather changes in cloud microphysical properties, since we do not see any significant change in updraft velocity from the clean to polluted condition with both SBM and Bulk.

[43] The averaged hydrometeor number and mass concentrations over the study region are shown in Figure 12. Since graupel/hail rarely exists in this SC case in the model simulations (also no ice-containing precipitation was observed at the surface), it is not shown in the figure and excluded for further discussion. The most striking difference between SBM and Bulk is again in simulating droplet and raindrop number concentrations, similar to the previous DCC case. Under the clean condition, Bulk predicts up to 5 times higher N_c but 10 times higher N_r than SBM. In the polluted case, Bulk predicts over 3–5 times higher N_c but similar N_r. Differences of N_c between SBM and Bulk are much larger for this SC than for the DCC under the polluted condition. As discussed in the section for the DCC, the very high N_c with Bulk even in

Table 3b. Quantities Averaged Over the Large Region (30.5°N–33.8°N and 113.5°E–117.5°E), i.e., 3-D Domain Average, for SC in Nov 07 (LST)

	P_sbm	C_sbm	P_bulk	C_bulk	Changes With SBM (%)	Changes With Bulk (%)
N_c (cm^{-3})	8.83	1.72	53.88	12.25	413.9	339.9
N_r (L^{-1})	0.93	1.26	1.04	6.06	−26.2	−82.8
N_i (L^{-1})	15.26	13.26	9.47	9.40	15.1	0.67
Q_c (g kg^{-1})	0.031	0.025	0.044	0.034	24.0	29.4
Q_r (g kg^{-1})	0.018	0.02	0.011	0.016	−10.0	−31.3
Q_i (g kg^{-1})	0.019	0.0185	0.0163	0.0159	2.7	2.5
Precipitation (mm)	3.56	3.74	3.52	3.58	−4.76	−1.59

the clean case (N_c in the C_Bulk is even higher than that in P_sbm) is mainly because CCN are fixed everywhere during the simulation, which is unrealistic. N_r in Bulk is highly uncertain, as it is affected by many factors discussed in Section 4.1.3. Q_c is increased in the polluted case, similar to that in the DCC and both SBM and Bulk are consistent with each other on this point. Q_r is decreased by the increase of CCN with both SBM and Bulk for this SC (for the DCC, it is increased with SBM but decreased with Bulk). The much higher N_c in P_bulk relative to C_bulk results in over 30% reduction of mean droplet size by increasing CCN, much more significant than that with SBM. In this SC, SBM and Bulk qualitatively agree with each other in the CCN effects on the properties of droplet and raindrop, but Bulk does predict much larger CCN effects relative to SBM mainly due to the fixed CCN in Bulk.

[44] We do not see significant CCN effects on ice microphysical properties such as N_i and Q_i with both SBM and Bulk in this cloud case. It is not surprising that the effect of CCN on ice microphysical properties is small in this type of clouds because condensation/deposition freezing cannot change much by the very small change in cloud vertical velocity by CCN and droplet freezing is very inefficient in such warm cloud temperatures (above −15°C). However, N_i could be very different in the simulations of SBM and Bulk. For example, SBM predicts over 3 times higher N_i relative to Bulk during 0–6:00 LST, likely because higher supersaturation is produced for the deeper clouds during that period and the Meyer's parameterization employed in SBM tends to predict much higher ice crystal concentrations than *Cooper* [1986] used in Bulk at a certain supersaturation over the temperature range of −5 to −25°C [*Rasmussen et al.*, 2002]. The decreased Q_r and not much change of Q_i by CCN explain the reduced precipitation in this SC, with both SBM and Bulk.

[45] Averaged over the large region, the differences in precipitation and hydrometeor number and mass concentrations between SBM and Bulk do not qualitatively change compared to analysis over the study region. As shown in Table 3b, Bulk and SBM predict similar precipitation under both clean and polluted condition. Bulk predicts significantly higher N_c and N_r than SBM, especially under the clean condition. In addition, CCN effects on the cloud microphysical properties and the accumulated precipitation do not change qualitatively either: an increase in CCN increases N_c and decreases N_r and precipitation; Bulk predicts very small changes of ice microphysical properties. Since heavy rain occurs much more often over the large region relative to the small region we discussed previously, the reduction in heavy rain amount by the increase of CCN in Bulk should be robust and it is consistent with the SBM simulations.

5. Conclusions and Discussion

[46] Two different cloud regimes – deep convective clouds and stratus clouds, observed during the AMF-China field campaign, are simulated using the WRF model with a spectral-bin microphysical scheme and a two-moment bulk microphysical scheme. For the first time, surface-based measurements of aerosol and cloud properties acquired in China are used to evaluate the model simulations and support modeling study of aerosol indirect effects. By contrasting simulations with a CCN level resembling the observed polluted environment and a CCN level that resembles the cleaner environment about 30–40 years ago, we examine the effects of aerosols on cloud microphysical properties and precipitation for two different cloud regimes. The simulated DCC and SC systems with SBM under the polluted condition generally agree with observations in terms of cloud evolution, rain pattern, and surface precipitation. On the contrary, with Bulk under the same CCN level, we see higher cloud top height, larger LWC and LWP, and earlier onset of precipitation for the DCC. In the stratiform cloud study with Bulk, the results also showed larger LWC and LWP and higher cloud top height, but lower rain rate and delay of the onset of precipitation.

[47] We find that the SBM and Morrison's bulk scheme predict consistent results in CCN effects on precipitation for the SC, but produce opposite results for the DCC. Specifically, both SBM and Bulk predict reduced precipitation when CCN are increased by 6 times for the SC. For the DCC, with SBM, the increase in CCN invigorates the DCC in which wind shear is weak, resulting in stronger convection, a larger frequency of heavy rain and more accumulated precipitation. However, Bulk is not able to simulate the invigoration effect of CCN, i.e., it predicts weaker convection and reduced precipitation in the polluted case. Although Bulk also predicts smaller rain occurrence frequency and amount for light and intermediate rain as SBM, it predicts little change in frequency and amount for heavy rain from the clean to the polluted case, while SBM estimates an increase by over 20%. The reduced frequency and amount for light rain but enhanced ones for heavy rain in the polluted case predicted by SBM are also found in analyses of the observed decadal trend over the region [*Qian et al.*, 2009]. With Bulk, stronger droplet nucleation due to strong convection and the fixed CCN result in much higher droplet

number and substantially smaller droplet size in the polluted environment. As a result, latent heat release is reduced because of the reduced ice mass, leading to the suppressed convection. Our sensitivity tests indicate that the much higher N_c and the opposite CCN effects on convection and heavy rain with Bulk compared to SBM stem from too strong droplet nucleation with the fixed CCN in Bulk.

[48] An increase in CCN increases N_c but decreases N_r in the both DCC and SC, and both SBM and Bulk agree with each other. The most striking difference is that Bulk predicts much higher N_c in the polluted air and much higher N_r in the clean air compared to SBM. The much higher N_c with Bulk than SBM is mainly due to the fixed CCN. We tested a prognostic CCN approach for the DCC case that simulated N_c much closer to that of SBM. Our sensitivity tests also indicate that the much smaller cutoff size in distinguishing droplet and raindrop and the assumed smaller size for newly formed raindrop (i.e., 25 μm) are factors that significantly contribute to the higher N_r with Bulk. CCN have less significant effects on ice microphysical properties with Bulk than SBM. The higher sensitivity of ice formation to supersaturation in the condensational/depositional freezing parameterization used in SBM could contribute to it. Riming is uncertain in Bulk because of the simple parameterization that assumes a constant riming efficiency. Conversion of particles to graupel and hail is uncertain in both Bulk and SBM since it is based on particle size or mixing ratio thresholds that have a limited physical basis. New approaches that predict rimed mass fraction [*Morrison and Grabowski*, 2008, 2010] and spectral ice habits [*Hashino and Tripoli*, 2007] provide an improved physical basis for parameterizing conversion to graupel in both bin and bulk schemes.

[49] In summary, for either Bulk or SBM applied to both DCC and SC, increasing CCN increases cloud droplet number and mass concentrations, decreases raindrop number concentration, and delays the onset of precipitation. The increase of CCN significantly changes the spatial and temporal distributions of precipitation and cloud base and top heights for the DCC but has little effect on them for the SC. Other features that SBM and Bulk agree for the SC include: increasing CCN does not change rain frequency much but reduces rain amount significantly; it does not evidently affect ice microphysical properties because condensation/deposition freezing change little with small changes of vertical velocity by CCN and droplet freezing is inefficient.

[50] Although Bulk and SBM agree on some aspects of aerosol effects, differences in many quantities such as convective strength and liquid microphysical properties between SBM and Bulk with the same initial CCN are much larger than the CCN effects simulated with each scheme, suggesting that large uncertainty can be introduced by cloud microphysical parameterization in cloud and climate simulations. Our study also shows that fixed CCN, which is commonly employed in bulk schemes used in many cloud and regional and global climate simulations, can produce significant deviation in cloud properties and severely affect the sensitivity of deep convection to changes of aerosols, as also seen in work by *Ekman et al.* [2011]. Some studies of aerosol effects did not even include CCN (i.e., cloud droplet concentration is prescribed and fixed). As shown in this study, the modified Bulk with prognostic CCN shows a much better agreement in N_c and CCN effects on convection with SBM. This is very important for studying AIE in the DCC. Other potential areas of improvement include employing better representations of autoconversion of cloud droplets to raindrops, and ice to snow, which have large effects on precipitation. The riming rate from rain-ice (snow) collision, which is simply parameterized using a constant in bulk schemes, should be validated using SBM since collection efficiencies are not well-constrained by observations. In the follow-on paper, we will detail all of the improvements that we make and extensively evaluate the bulk scheme using SBM.

[51] **Acknowledgments.** This study was supported by the U.S. DOE's Office of Science Biological and Environmental Research under a bilateral agreement with the China Ministry of Sciences and Technology on regional climate research. PNNL is operated for the U.S. DOE by Battelle Memorial Institute under Contract DE-AC06-76RLO1830. We appreciate the help on WRF from Jimy Dudhia at NCAR, Bill Gustafson at PNNL and Amy Solomon at NOAA. We have benefited greatly from interactions with Barry Lynn and Alexander Khain of the Hebrew University of Jerusalem on improvements to WRF-SBM. The DOE ARM infrastructure is acknowledged for obtaining the data, and we thank Maria Cadeddu from Argonne National Laboratory for providing information on the uncertainty of MWRP data. We appreciate four anonymous reviewers for their comments that help improved the manuscript.

References

Ackerman, A. S., M. P. Kirkpatrick, D. E. Stevens, and O. B. Toon (2004), The impact of humidity above stratiform clouds on indirect aerosol climate forcing, *Nature*, *432*, 1014–1017, doi:10.1038/nature03174.

Andreae, M. O., et al. (2004), Smoking rain clouds over the Amazon, *Science*, *303*, 1337–1342, doi:10.1126/science.1092779.

Beheng, K. D. (1994), A parameterization of warm cloud microphysical conversion processes, *Atmos. Res.*, *33*, 193–206, doi:10.1016/0169-8095(94)90020-5.

Bigg, E. K. (1953), The formation of atmospheric ice crystals by the freezing of droplets, *Q. J. R. Meteorol. Soc.*, *79*, 510–519, doi:10.1002/qj.49707934207.

Cheng, Y.-J., J.-H. Zhang, Y.-F. Luo, Z.-T. Liu, G. Lesins, and U. Lohmann (2005), Contribution of changes in sea surface temperature and aerosol loading to the decreasing precipitation trend in southern China, *J. Clim.*, *18*, 1381–1390, doi:10.1175/JCLI3341.1.

Cooper, W. A. (1986), Ice initiation in natural clouds, *Meteorol. Monogr.*, *43*, 29–32.

Ekman, A. M. L., A. Engstrom, and A. Soderberg (2011), Impact of two-way aerosol-cloud interaction and changes in aerosol size distribution on simulated aerosol-induced deep convective cloud sensitivity, *J. Atmos. Sci.*, *68*, 685–698, doi:10.1175/2010JAS3651.1.

Fan, J., R. Zhang, G. Li, W.-K. Tao, and X. Li (2007a), Simulations of cumulus clouds using a spectral microphysics cloud-resolving model, *J. Geophys. Res.*, *112*, D04201, doi:10.1029/2006JD007688.

Fan, J., R. Zhang, G. Li, and W.-K. Tao (2007b), Effects of aerosols and relative humidity on cumulus clouds, *J. Geophys. Res.*, *112*, D14204, doi:10.1029/2006JD008136.

Fan, J., M. Ovtchinnikov, J. Comstock, S. McFarlane, and A. Khain, (2009a), Ice formation in Arctic mixed-phase clouds: Insights from a 3-D cloud-resolving model with size-resolved aerosol and cloud microphysics, *J. Geophys. Res.*, *114*, D04205, doi:10.1029/2008JD010782.

Fan, J., T. Yuan, J. M. Comstock, S. Ghan, A. Khain, L. R. Leung, Z. Li, V. J. Martins, and M. Ovchinnikov (2009b), Dominant role by vertical wind shear in regulating aerosol effects on deep convective clouds, *J. Geophys. Res.*, *114*, D22206, doi:10.1029/2009JD012352.

Fan, J., et al. (2010a), Tropical anvil characteristics and water vapor of the tropical tropopause layer: Impact of heterogeneous and homogeneous freezing parameterizations, *J. Geophys. Res.*, *115*, D12201, doi:10.1029/2009JD012696.

Fan, J., J. M. Comstock, and M. Ovchinnikov (2010b), The cloud condensation nuclei and ice nuclei effects on tropical anvil characteristics and water vapor of the tropical tropopause layer, *Environ. Res. Lett.*, *5*, 044005, doi:10.1088/1748-9326/5/4/044005.

Feingold, G., and S. M. Kreidenweis (2002), Cloud processing of aerosol as modeled by a large eddy simulation with coupled microphysics and aqueous chemistry, *J. Geophys. Res.*, *107*(D23), 4687, doi:10.1029/2002JD002054.

Gao, J., et al. (2007), Number concentration and size distributions of submicron particles in Jinan urban area: Characteristics in summer and winter, *J. Environ. Sci.*, *19*, 1466–1473, doi:10.1016/S1001-0742(07)60239-3.

Guo, H., Y. Liu, and J. E. Penner (2008), Does the threshold representation associated with the autoconversion process matter?, *Atmos. Chem. Phys.*, *8*, 1225–1230, doi:10.5194/acp-8-1225-2008.

Harrington, J. Y., M. P. Meyers, R. L. Walko, and W. R. Cotton (1995), Parameterization of ice crystal conversion process due to vapor deposition for mesoscale models using double moment basis functions. Part I: Basic formulation and parcel model results, *J. Atmos. Sci.*, *52*, 4344–4366, doi:10.1175/1520-0469(1995)052<4344:POICCP>2.0.CO;2.

Hashino, T., and G. J. Tripoli (2007), The Spectral Ice Habit Prediction System (SHIPS). Part I: Model description and simulation of the vapor deposition, *J. Atmos. Sci.*, *64*, 2210–2237, doi:10.1175/JAS3963.1.

Huang, Y., W. L. Chameides, and R. E. Dickinson (2007), Direct and indirect effects of anthropogenic aerosols on regional precipitation over east Asia, *J. Geophys. Res.*, *112*, D03212, doi:10.1029/2006JD007114.

Iguchi, T., T. Nakajima, A. P. Khain, K. Saito, T. Takemura, and K. Suzuki (2008), Modeling the influence of aerosols on cloud microphysical properties in the east Asia region using a mesoscale model coupled with a bin-based cloud microphysics scheme, *J. Geophys. Res.*, *113*, D14215, doi:10.1029/2007JD009774.

Kaufman, Y. J., I. Koren, L. A. Remer, D. Rosenfeld, and Y. Rudich (2005), The effect of smoke, dust, and pollution aerosol on shallow cloud development over the Atlantic Ocean, *Proc. Natl. Acad. Sci. U. S. A.*, *102*, 11,207–11,212, doi:10.1073/pnas.0505191102.

Khain, A., and B. Lynn (2009), Simulation of a supercell storm in clean and dirty atmosphere using weather research and forecast model with spectral bin microphysics, *J. Geophys. Res.*, *114*, D19209, doi:10.1029/2009JD011827.

Khain, A., and A. Pokrovsky (2004), Simulation of effects of atmospheric aerosols on deep turbulent convective clouds using a spectral microphysics mixed-phase cumulus cloud model. Part II: Sensitivity study, *J. Atmos. Sci.*, *61*, 2983–3001.

Khain, A. P., M. Ovtchinnikov, M. Pinsky, A. Pokrovsky, and H. Krugliak (2000), Notes on the state-of-the-art numerical modeling of cloud microphysics, *Atmos. Res.*, *55*, 159–224, doi:10.1016/S0169-8095(00)00064-8.

Khain, A. P., et al. (2004), Simulation of effects of atmospheric aerosols on deep turbulent convective clouds using a spectral microphysics mixed-phase cumulus cloud model. Part I: Model description and possible applications, *J. Atmos. Sci.*, *61*, 2963–2982, doi:10.1175/JAS-3350.1.

Khain, A. P., D. Rosenfeld, and A. Pokrovsky (2005), Aerosol impact on the dynamics and microphysics of deep convective clouds, *Q. J. R. Meteorol. Soc.*, *131*, 2639–2663, doi:10.1256/qj.04.62.

Khain, A. P., N. BenMoshe, and A. Pokrovsk (2008), Factors determining the impact of aerosols on surface precipitation from clouds: Attempt of classification, *J. Atmos. Sci.*, *65*, 1721–1748, doi:10.1175/2007JAS2515.1.

Khain, A., L. R. Leung, B. Lynn, and S. Ghan (2009), Effects of aerosols on the dynamics and microphysics of squall lines simulated by spectral bin and bulk parameterization schemes, *J. Geophys. Res.*, *114*, D22203, doi:10.1029/2009JD011902.

Khain, A., B. Lynn, and J. Dudhia (2010), Aerosol effects on intensity of landfalling hurricanes as seen from simulations with the WRF model with spectral bin microphysics, *J. Atmos. Sci.*, *67*, 365–384, doi:10.1175/2009JAS3210.1.

Khairoutdinov, M., and Y. Kogan (2000), A new cloud physics parameterization in a large-eddy simulation model of marine stratocumulus, *Mon. Weather Rev.*, *128*, 229–243, doi:10.1175/1520-0493(2000)128<0229:ANCPPI>2.0.CO;2.

Kogan, Y. (1991), The simulation of a convective cloud in a 3-D model with explicit microphysics. Part 1: Model description and sensitivity experiments, *J. Atmos. Sci.*, *48*, 1160–1189, doi:10.1175/1520-0469(1991)048<1160:TSOACC>2.0.CO;2.

Koren, I., J. V. Martins, L. A. Remer, and H. Afargan (2008), Smoke invigoration versus inhibition of clouds over the Amazon, *Science*, *321*, 946, doi:10.1126/science.1159185.

Levin, Z., and W. Cotton (Eds.) (2008), *Aerosol Pollution Impact on Precipitation: A Scientific Review*, Springer, New York.

Li, G., Y. Wang, and R. Zhang (2008), Implementation of a two-moment bulk microphysics scheme to the WRF model to investigate aerosol-cloud interaction, *J. Geophys. Res.*, *113*, D15211, doi:10.1029/2007JD009361.

Li, X., W.-K. Tao, A. P. Khain, J. Simpson, and D. E. Johnson (2009), Sensitivity of a cloud-resolving model to bulk and explicit bin microphysical schemes. Part 2: Cloud microphysics and storm dynamics interaction, *J. Atmos. Sci.*, *66*, 22–40, doi:10.1175/2008JAS2647.1.

Li, Z., et al. (2007), Preface to special section: Overview of the East Asian Study of Tropospheric Aerosols: An International Regional Experiment (EAST-AIRE), *J. Geophys. Res.*, *112*, D22S00, doi:10.1029/2007JD008853.

Li, Z., K.-H. Lee, J. Xin, Y. Wang, and W.-M. Hao (2010), First observation-based estimates of aerosol radiative forcing at the top, bottom and inside of the atmosphere, *J. Geophys. Res.*, *115*, D00K18, doi:10.1029/2009JD013306.

Li, Z., et al. (2011), East Asian Studies of Tropospheric Aerosols and their Impact on Regional Climate (EAST-AIRC): An overview, *J. Geophys. Res.*, *116*, D00K34, doi:10.1029/2010JD015257.

Li, Z., F. Niu, J. Fan, Y. Liu, D. Rosenfeld, and Y. Ding (2012), Long-term impact of aerosols on the vertical development of cloud and precipitation, *Nat. Geosci.*, doi:10.1038/ngeo1313, in press.

Lin, J. C., T. Matsui, R. A. Pielke Sr., and C. Kummerow (2006), Effects of biomass-burning-derived aerosols on precipitation and clouds in the Amazon Basin: A satellite-based empirical study, *J. Geophys. Res.*, *111*, D19204, doi:10.1029/2005JD006884.

Liu, J., Y. Zheng, C. Flynn, M. Cribb (2012), Seasonal variations of aerosol optical properties, vertical distribution and associated radiative effects in the Yangtze Delta Region of China, *J. Geophys. Res.*, doi:10.1029/2011JD016490, in press.

Loeb, N. G., and G. L. Schuster (2008), An observational study of the relationship between cloud, aerosol and meteorology in broken low-level cloud conditions, *J. Geophys. Res.*, *113*, D14214, doi:10.1029/2007JD009763.

Lynn, B., and A. Khain (2007), Utilization of spectral bin microphysics and bulk parameterization schemes to simulate the cloud structure and precipitation in a mesoscale rain event, *J. Geophys. Res.*, *112*, D22205, doi:10.1029/2007JD008475.

Lynn, B. H., et al. (2005a), Spectral (Bin) microphysics coupled with a mesoscale model (MM5). Part I: Model description and first results, *Mon. Weather Rev.*, *133*, 44–58.

Lynn, B. H., et al. (2005b), Spectral (Bin) microphysics coupled with a mesoscale model (MM5). Part II: Simulation of a CaPE rain event with a squall line, *Mon. Weather Rev.*, *133*, 59–71.

Meyers, M. P., P. J. DeMott, and W. R. Cotton (1992), New primary ice-nucleation parameterizations in an explicit cloud model, *J. Appl. Meteorol.*, *31*, 708–721, doi:10.1175/1520-0450(1992)031<0708:NPINPI>2.0.CO;2.

Morrison, H., and W. W. Grabowski (2008), A novel approach for representing ice microphysics in models: Description and tests using a kinematic framework, *J. Atmos. Sci.*, *65*, 1528–1548, doi:10.1175/2007JAS2491.1.

Morrison, H., and W. W. Grabowski (2010), An improved representation of rimed snow and conversion to graupel in a mutlicomponent bin microphysics scheme, *J. Atmos. Sci.*, *67*, 1337–1360, doi:10.1175/2010JAS3250.1.

Morrison, H., and J. O. Pinto (2005), Mesoscale modeling of springtime Arctic mixed-phase stratiform clouds using a new two-moment bulk microphysics scheme, *J. Atmos. Sci.*, *62*, 3683–3704.

Morrison, H., J. A. Curry, and V. I. Khvorostyanov (2005), A new double-moment microphysics parameterization for application in cloud and climate models. Part I: Description, *J. Atmos. Sci.*, *62*, 1665–1677, doi:10.1175/JAS3446.1.

Morrison, H., G. Thompson, and V. Tatarskii (2009), Impact of cloud microphysics on the development of trailing stratiform precipitation in a simulated squall line: Comparison of one- and two-moment schemes, *Mon. Weather Rev.*, *137*, 991–1007, doi:10.1175/2008MWR2556.1.

Muhlbauer, A., et al. (2010), Intercomparison of aerosol-cloud-precipitation interactions in stratiform orographic mixed-phase clouds, *Atmos. Chem. Phys.*, *10*, 8173–8196, doi:10.5194/acp-10-8173-2010.

National Research Council (2005), *Radiative Forcing of Climate Change: Expanding the Concept and Addressing Uncertainties*, Natl. Acad. Press, Washington, D. C.

Pinsky, M., and A. Khain (1998), Some effects of cloud turbulence on water–ice and ice–ice collisions, *Atmos. Res.*, *47–48*, 69–86, doi:10.1016/S0169-8095(98)00041-6.

Pinsky, M., A. Khain, and M. Shapiro (2000), Stochastic effects on cloud droplet hydrodynamic interaction in a turbulent flow, *Atmos. Res.*, *53*, 131–169, doi:10.1016/S0169-8095(99)00048-4.

Pruppacher, H. R., and J. D. Klett (1997), *Microphysics of Clouds and Precipitation*, 2nd ed., Springer, New York.

Qian, Y., L. R. Leung, S. J. Ghan, and F. Giorgi (2003), Regional climate effects of aerosols over China: Modeling and observation, *Tellus, Ser. B*, *55*(4), 914–934, doi:10.1046/j.1435-6935.2003.00070.x.

Qian, Y., D. P. Kaiser, L. R. Leung, and M. Xu (2006), More frequent cloud-free sky and less surface solar radiation in China from 1955 to 2000, *Geophys. Res. Lett.*, *33*, L01812, doi:10.1029/2005GL024586.

Qian, Y., D. Gong, J. Fan, L. R. Leung, R. Bennartz, D. Chen, and W. Wang (2009), Heavy pollution suppresses light rain in China: Observations and modeling, *J. Geophys. Res.*, *114*, D00K02, doi:10.1029/2008JD011575.

Rasmussen, R. M., I. Geresdi, G. Thompson, K. Manning, and E. Karplus (2002), Freezing drizzle formation in stably stratified layer clouds: The role of radiative cooling of cloud droplets, cloud condensation nuclei, and ice initiation, *J. Atmos. Sci.*, *59*, 837–860, doi:10.1175/1520-0469(2002)059<0837:FDFISS>2.0.CO;2.

Rogers, R. R., and M. K. Yau (1989), Formation of cloud droplets, in *A Short Course in Cloud Physics*, 3rd ed., pp. 94–95, Pergamon, New York.

Rosenfeld, D. (2000), Suppression of rain and snow by urban and industrial air pollution, *Science*, *287*, 1793–1796, doi:10.1126/science.287.5459.1793.

Rosenfeld, D., J. Dai, X. Yu, Z. Yao, X. Xu, X. Yang, and C. Du (2007), Inverse relations between amounts of air pollution and orographic precipitation, *Science*, *315*, 1396–1398, doi:10.1126/science.1137949.

Rosenfeld, D., U. Lohmann, G. B. Raga, C. D. O'Dowd, M. Kulmala, S. Fuzzi, A. Reissell, and M. O. Andreae (2008), Flood or drought: How do aerosols affect precipitation?, *Science*, *321*, 1309–1313, doi:10.1126/science.1160606.

Seifert, A. (2008), On the parameterization of evaporation of raindrops as simulated by a one-dimensional rainshaft model, *J. Atmos. Sci.*, *65*, 3608, doi:10.1175/2008JAS2586.1.

Seifert, A., and K. D. Beheng (2001), A double-moment parameterization for simulating autoconversion, accretion, and self-collection, *Atmos. Res.*, *59–60*, 265–281, doi:10.1016/S0169-8095(01)00126-0.

Seifert, A., et al. (2006), Comparison of spectral bin and two-moment bulk mixed-phase cloud microphysics, *Atmos. Res.*, *80*, 46–66.

Skamarock, W. C., J. B. Klemp, J. Dudhia, D. O. Gill, D. M. Barker, W. Wang, and J. G. Powers (2005), A description of the advanced research WRF version 2, *NCAR Tech. Note NCAR/TN-468+STR*, 88 pp., Natl. Cent. for Atmos. Res., Boulder, Colo.

Solomon, A., et al. (2009), Investigation of microphysical parameterizations of snow and ice in Arctic clouds during M-PACE through model–observation comparisons, *Mon. Weather Rev.*, *137*, 3110–3128, doi:10.1175/2009MWR2688.1.

Stevens, B., and G. Feingold (2009), Untangling aerosol effects on clouds and precipitation in a buffered system, *Nature*, *461*, 607–613, doi:10.1038/nature08281.

Tao, W.-K., X. Li, A. Khain, T. Matsui, S. Lang, and J. Simpson (2007), Role of atmospheric aerosol concentration on deep convective precipitation: Cloud-resolving model simulations, *J. Geophys. Res.*, *112*, D24S18, doi:10.1029/2007JD008728.

Twomey, S. (1959), The nuclei of natural cloud formation: II. The supersaturation in natural clouds and the variation of cloud droplet concentration, *Geofis. Pura Appl.*, *43*, 243–249, doi:10.1007/BF01993560.

van den Heever, S. C., G. G. Carrio, W. R. Cotton, P. J. DeMott, and A. J. Prenni (2006), Impact of nucleating aerosol on Florida storms, part 1: Mesoscale simulations, *J. Atmos. Sci.*, *63*, 1752–1775, doi:10.1175/JAS3713.1.

Wang, C. (2005), A modeling study of the response of tropical deep convection to the increase of cloud condensation nuclei concentration: 1. Dynamics and microphysics, *J. Geophys. Res.*, *110*, D21211, doi:10.1029/2004JD005720.

Yao, C., S. Yang, W. Qian, Z. Lin, and M. Wen (2008), Regional summer precipitation events in Asia and their changes in the past decades, *J. Geophys. Res.*, *113*, D17107, doi:10.1029/2007JD009603.

Young, K. C. (1974), The role of contact nucleation in ice phase initiation in clouds, *J. Atmos. Sci.*, *31*, 768–780.

Yuan, T., Z. Li, R. Zhang, and J. Fan (2008), Increase of cloud droplet size with aerosol optical depth: An observation and modeling study, *J. Geophys. Res.*, *113*, D04201, doi:10.1029/2007JD008632.

Zhang, R., G. Li, J. Fan, D. L. Wu, and M. J. Molina (2007), Intensification of Pacific storm track linked to Asian pollution, *Proc. Natl. Acad. Sci. U. S. A.*, *104*, 5295–5299, doi:10.1073/pnas.0700618104.

Zhao, C., X. Tie, and Y. Lin (2006), A possible positive feedback of reduction of precipitation and increase in aerosols over eastern central China, *Geophys. Res. Lett.*, *33*, L11814, doi:10.1029/2006GL025959.

Zhou, Y., et al. (2008), Retrieval and preliminary test of cloud physical parameters from combination of FY22C/D geostationary satellite data and other observation data, *Meteorol. Mon.*, *34*(12), 27–35.

H. Chen, Institute of Atmospheric Physics, Chinese Academy of Sciences, Beijing 100029, China.

J. Fan, R. Leung, and Y. Qian, Atmospheric Sciences and Global Change Division, Pacific Northwest National Laboratory, Richland, WA 99352, USA. (jiwen.fan@pnl.gov)

Z. Li, Department of Atmospheric and Oceanic Sciences, University of Maryland, College Park, MD 20740, USA.

H. Morrison, Mesoscale and Microscale Meteorology Division, National Center for Atmospheric Research, Boulder, CO 80307, USA.

Y. Wang, Department of Atmospheric Sciences, Texas A&M University, College Station, TX 77801, USA.

Y. Zhou, Weather Modification Centre, Chinese Academy of Meteorological Sciences, Beijing 100081, China.